

# Fermionic greybody factors in dilaton black holes

Jahed Abedi<sup>1</sup> and Hessamaddin Arfaei<sup>1,2</sup>

<sup>1</sup> Department of Physics, Sharif University of Technology,  
P.O. Box 11155-9161, Tehran, Iran

<sup>2</sup> School of Particles and Accelerators,  
Institute for Research in Fundamental Sciences (IPM),  
P.O. Box 19395-5531, Tehran, Iran

E-mail: jahed\_abedi@physics.sharif.ir, arfaei@ipm.ir

**Abstract.** In this paper the question of emission of fermions in the process of dilaton black hole evolution and its characters for different dilaton coupling constants  $\alpha$  is studied. The main quantity of interest, the greybody factors are calculated both numerically and in analytical approximation. The dependence of rates of evaporation and behaviour on the dilaton coupling constant is analyzed. Having calculated the greybody factors we are able to address the question of the final fate of the dilaton black hole. For that we also need to make dynamical treatment of the solution by considering the backreaction which will show a crucial effect on the final result. We find a transition line in  $(Q/M, \alpha)$  plane that separates the two regimes for the fate of the black hole, decay regime and extremal regime. In the decay regime the black hole completely evaporates, while in the extremal regime the black hole approaches the extremal limit by radiation and becomes stable.

**Keywords:** black hole, dilaton, Hawking radiation, backreaction, fate of a black hole, greybody factors, fermion

PACS numbers: 04.70.Dy, 04.60.Cf, 04.70.Bw

## 1. Introduction

Gravitational systems coupled to Maxwell and dilaton fields emerge from several more fundamental theories. In particular the low energy limit of (super) string theory or Kaluza-Klein compactifications result in such systems, which have been studied for long time [1–4]. Corresponding black holes and their evaporation are also studied previously. The exact black hole solution goes back to [5, 7] from 70’s. The thermodynamics of the black hole in this theory shows interesting properties which depend on the dilaton coupling  $\alpha$ . For  $\alpha < 1$  one expects similar properties as for the standard Reissner-Nordström black hole, although we find a range  $1/\sqrt{3} \leq \alpha < 1$  in which some properties differ significantly. The behaviour of the theory in the range of  $\alpha > 1$  is significantly different and shows unexpected features some of which are addressed in this article. The particle emission by dilaton black holes studied in several articles falls among them. Holzhey and Wilczek [3] derived the potential barrier which for  $\alpha > 1$  strongly impedes the particle radiation to the extent that may stop it. In contrast, Koga and Maeda [4] showed by numerical computation that Hawking radiation wins over the barrier and the dilaton black hole does not stop radiating, despite the fact that the potential barrier becomes infinitely high. All this is done for emission of scalars and in semi-classical approximation. The question is which of these results stay valid once we consider the process for fermions and consider next order correction arising from the back-reaction. As expected, fermionic emission show more or less similar properties qualitatively as scalars, but considering next order of dynamical effect as back-reaction changes the scene and becomes the key factor when the evolution of the black hole moves it close to the extremal limit.

Shortly after the discovery of Hawking radiation, it was noticed that due to large value of  $\frac{e}{m} \simeq 2 \times 10^{21}$ , large black holes are unlikely to hold any charge and rapidly radiate away their charges [6] and become neutral. Hence in nature we must look for neutral black holes rather than charged ones. However, considering the next order effect of the dynamics of the dilaton black hole we find that this need not be valid for all ranges of parameters. We find a transition line in the  $(Q/M, \alpha)$  plane which designates the border between two regions; one region specifies the parameters for black holes which evaporate completely and the other for black holes that end up as extremal condition. In the latter case the black hole stops radiating and becomes stable.

The radiation rates of spin 1/2 particles and the fate of different types of Einstein Hilbert black-holes in the semi-classical approximation [8–17] using greybody factors have been calculated both numerically and analytically. Certain results on the scattering parameters of Dirac field such as quasinormal frequencies or decay rates in the background of dilaton [18, 19] and other types of black holes are also presented [20–38]. But there are number of unsettled questions which we will consider in this article.

For completeness and setting the notation the next section is devoted to a quick review of the charged dilaton black hole and its properties, such as general results on

decay rates of mass and charge, thermodynamics, etc.

In section 3 we set up the Dirac equations for emission of charged fermions in the background of a charged dilaton black hole and derive the effective potentials. We also solve the equations to find the greybody factors that are the important factors in calculation of the emission rates.

Our main results which are obtained by numerical computations are presented in section 4, but to get a better view we also look at analytical approximation of the solutions to the Dirac equations and evaluation of the greybody factors using Rosen-Morse potential [39–41] and WKB approximation. The evolution of the charged dilaton black hole and the rates of charge and mass emission are discussed and the existence of a transition line is demonstrated. We also compute the transition line for different ranges of the parameters of the problem at hand.

Section 5 is devoted to the analysis of the results and their behaviour under change of various parameters involved.

Finally in section 6 we end with concluding remarks and future plans. In the appendix the details of the computation of the effective potential for fermions in the background of most general static black hole is presented.

## 2. A short review of dilaton black hole, greybody factors and Hawking radiation

In this section we consider an Einstein-Maxwell gravity coupled to a dilaton field  $\phi$  with the dilaton coupling constant  $\alpha$ . The action is

$$S = \int d^4x \sqrt{-g} [R - 2(\nabla\phi)^2 + e^{-2\alpha\phi} F^2]. \quad (2.1)$$

The signature of the metric is  $(+ - - -)$ . The parameter  $\alpha$  is a dimensionless constant, and  $F^2 = F_{\mu\nu} F^{\mu\nu}$ . The behaviour of the theory shows non-trivial dependence on  $\alpha$  that we will see in rest of the article. The equations of motion are;

the Maxwell equations

$$\nabla_\mu (e^{-2\alpha\phi} F^{\mu\nu}) = 0, \quad (2.2)$$

$$\partial_{[\rho} F_{\mu\nu]} = 0, \quad (2.3)$$

the Einstein equations

$$R_{\mu\nu} = e^{-2\alpha\phi} (-2F_{\mu\rho} F_\nu^\rho + \frac{1}{2} F^2 g_{\mu\nu}) + 2\partial_\mu \phi \partial_\nu \phi, \quad (2.4)$$

and the dilaton equation

$$g^{\mu\nu} \nabla_\mu \nabla_\nu \phi = \frac{1}{2} \alpha e^{-2\alpha\phi} F^2. \quad (2.5)$$

The spherically symmetric black hole solutions of this action are well known and found long ago [1, 2];

$$ds^2 = f(r)^2 dt^2 - \frac{dr^2}{f(r)^2} - R(r)^2 d\Omega^2, \quad (2.6)$$

where

$$f(r)^2 = \left(1 - \frac{r_+}{r}\right) \left(1 - \frac{r_-}{r}\right)^{\frac{1-\alpha^2}{1+\alpha^2}}, \quad (2.7)$$

and

$$R(r)^2 = r^2 \left(1 - \frac{r_-}{r}\right)^{\frac{2\alpha^2}{1+\alpha^2}}. \quad (2.8)$$

The Maxwell and dilaton fields of the solution are,  $A_\mu = (A_t, 0, 0, 0)$ ,  $A_t = -\frac{Q}{r}$ , with

$$F_{tr} = \frac{e^{2\alpha\phi} Q}{R(r)^2}, \quad (2.9)$$

and

$$e^{2\alpha\phi} = \left(1 - \frac{r_-}{r}\right)^{\frac{2\alpha^2}{1+\alpha^2}}. \quad (2.10)$$

The two (inner and outer) horizons are located at

$$r_+ = M + \sqrt{M^2 - (1 - \alpha^2)Q^2}, \quad (2.11)$$

and

$$r_- = \frac{1 + \alpha^2}{1 - \alpha^2} (M - \sqrt{M^2 - (1 - \alpha^2)Q^2}), \quad (2.12)$$

where  $M$  and  $Q$  are ADM mass and charge of this black hole respectively. Note that for  $\alpha < 1$  in order to preserve reality of the horizons one must have  $|Q/M| \leq \frac{1}{\sqrt{1-\alpha^2}}$ , but for  $\alpha > 1$  we do not have such restriction. We shall see that the different behaviour of the black hole for these two ranges of  $\alpha$  occurs also in several places. To have  $r_+ > r_-$  we must also have  $\frac{Q^2}{M^2} < 1 + \alpha^2$  and in the extremal limit where the two horizons coincide;

$$\frac{Q^2}{M^2} = 1 + \alpha^2. \quad (2.13)$$

The case of  $r_- > r_+$  or equivalently  $\frac{Q^2}{M^2} > 1 + \alpha^2$  is not considered in detail in this article. It requires particular attention since it behaves very differently and is under study by the authors.

The Hawking temperature of this dilaton black hole is

$$T_H = \frac{1}{4\pi r_+} \left(1 - \frac{r_-}{r_+}\right)^{\frac{1-\alpha^2}{1+\alpha^2}}. \quad (2.14)$$

This dilaton black hole demonstrates interesting thermodynamical properties not present in non dilatonic ones [3, 4, 42, 43]. Obviously, the behaviour of the temperature is drastically different from the normal Reissner-Nordström black hole. For  $\alpha < 1$ , it is much like that of RN black hole and approaches zero when the black hole becomes extremal. The drastic difference occurs for  $\alpha > 1$  and  $\alpha = 1$ . When  $\alpha > 1$ , at the extremal limit the temperature diverges, while for  $\alpha = 1$  it has a finite value  $T_H = 1/4\pi r_+$ . Such behaviour implies that the Hawking radiation might be quite different with strong dependence on the coupling constant  $\alpha$ .

The condition (2.13) arise if  $r_+$  is truly the outer horizon,  $r_+ > r_-$ . In this case the inner horizon  $r_-$  of this black hole has other interesting characteristics which is unique among black holes [3]. For non-zero  $\alpha$  and for extremal black holes the angular factor  $R$  in the metric (2.6) vanishes at the event horizon and the geometry becomes singular which must be resolved. However, there is no such a singularity for Reissner-Nordström black hole ( $\alpha = 0$ ). In the string frame ( $\alpha = 1$ ) this singularity completely disappears by rescaling the metric with the conformal factor. In this frame which is obtained by removing the singular scale factor  $(1 - \frac{r_-}{r})$  from Einstein frame metric (2.6), and in the extremal limit, and imposing the asymptotic constant value of the dilaton  $\phi_0 = 0$ , we have [2],

$$ds_{string}^2 = dt^2 - \left(1 - \frac{r_+}{r}\right)^{-2} dr^2 - r^2 d\Omega^2. \quad (2.15)$$

In the String frame the geometry of  $t = cte.$  surfaces for this metric is similar to that of Reissner-Nordström for  $t = cte.$  surfaces.

Contrary to Reissner-Nordström ( $\alpha = 0$ ) where for  $Q > M$  the geometry becomes complex and exposes the naked singularity at  $r = 0$ , for dilaton black hole ( $\alpha > 0$ ) inner horizon can pass the outer horizon  $r_- > r_+$  or we can have  $1 < \frac{Q}{M\sqrt{1+\alpha^2}} \leq \frac{1}{\sqrt{1-\alpha^4}}$  for  $0 < \alpha < 1$  or  $Q > M\sqrt{1+\alpha^2}$  for  $\alpha \geq 1$  and the geometry remains real [3]. This range of parameters, as stated above requires its own analysis which is under study and shall be reported separately.

Hawking radiation at the event horizon is exactly the black-body radiation [5]. However, before this radiation reaches the distant observer, it must pass the curved space-time around the black hole horizon [44, 45] which modifies it to a large extent. Therefore an observer located at far distance from the black hole observes a different spectrum than pure black body radiation. The geometry outside the event horizon apart from red-shifting the radiation also plays the role of a potential barrier, thus filters the Hawking radiation. The portion of the Hawking radiation passing the barrier, just goes under the red shift to infinity whereas the remainder is reflected back into the black hole. Hence, from viewpoint of infinite observer the space-time around the black hole, acts like a potential barrier and forces a deviation on blackbody spectrum. This deviation can be calculated by obtaining greybody factors from the scattering coefficients of the black hole.

Holzhey and Wilczek have obtained the potential for scalars,  $V_\eta$  that at the extremal limit is proportional to  $(1-r_+/r)^{2(1-\alpha^2)/(1+\alpha^2)}$  [3]. It is illuminating to write the potential as a product of two factors as in the following,

$$V_\eta = V_{\eta 1} V_{\eta 2}, \quad (2.16)$$

$$V_{\eta 1} = \left(1 - \frac{r_+}{r}\right) \left(1 - \frac{r_-}{r}\right)^{\frac{1-3\alpha^2}{1+\alpha^2}}, \quad (2.17)$$

$$V_{\eta 2} = \frac{1}{r^2} \left( l(l+1) + \frac{r_- r + r_+ r (1 + \alpha^2)^2 - (2 + \alpha^2) r_- r_+}{(1 + \alpha^2)^2 r^2} - \frac{\alpha^4 r_- (1 - \frac{r_+}{r})}{(1 + \alpha^2)^2 r (1 - \frac{r_-}{r})} \right). \quad (2.18)$$

Again the strong dependence on  $\alpha$  with three distinct behaviour for  $\alpha < 1$ ,  $\alpha = 1$  and  $\alpha > 1$  is visible. For  $\alpha < 1$  it is qualitatively like RN black hole, i.e.  $\alpha = 0$ : it tends to zero at the event horizon, increases to a maximum and as  $r$  becomes large tends to zero again. For the case  $\alpha = 1$ , the height of the potential barrier near extremal limit remains finite. For the class of black holes with  $\alpha > 1$  in the extremal limit the height of the potential barrier diverges on the event horizon. For non-extremal cases the height of potential barrier is finite, but its peak grows as  $(r_+ - r_-)^{-2(\alpha^2-1)/(\alpha^2+1)}$  as one approaches the extremal limit. The behavior of the potential can be better understood in the tortoise coordinates. In this case and at the extremal limit the tortoise coordinate in the event horizon is finite and the height of potential barrier increases by decrease in its width. Based on the behaviour of effective potential for  $\alpha > 1$  Holzhey and Wilczek [3] came to expect that as one approaches the extremal limit, the emission rate of the black hole tends to zero. However, later Koga and Maeda [4] under the assumption of conservation of the Black hole charge, showed that numerical calculations point to the emission of the large amount of energy for the scalars in the extremal limit due to the afore-mentioned divergence of the temperature.

Mass and charge evaporation rates of black hole in terms of radiation spectrum are given by [15],

$$-\frac{dM}{dt} = \int_m^\infty \frac{d\omega}{2\pi} \sum_{\text{mods } n, \text{ charge } q} \frac{\omega(1 - |R_n(\omega)|^2)}{\exp((\omega - q\Phi_H)/T_H) \pm 1}, \quad (2.19)$$

$$-\frac{dQ}{dt} = \int_m^\infty \frac{d\omega}{2\pi} \sum_{\text{mods } n, \text{ charge } q} \frac{q(1 - |R_n(\omega)|^2)}{\exp((\omega - q\Phi_H)/T_H) \pm 1}. \quad (2.20)$$

with the minus sign is for bosons and the plus sign is for fermions. The electrical potential of black hole on the event horizon  $\Phi_H = Q/r_+$ . For near extremal limit or for black hole with small mass where emission of the quanta of energy and charge alters the temperature of black hole significantly, one must take into account backreaction effects in the Hawking radiation spectrum [46]. For this purpose, substituting  $\omega$  with  $-dM$

and  $q$  with  $-dQ$  in above formula and using first law of black hole thermodynamics [7] we obtain the nonthermal spectrum of Hawking radiation,

$$-\frac{dM}{dt} = \int_m^\infty \frac{d\omega}{2\pi} \sum_{\text{mods } n, \text{ charge } q} \frac{\omega(1 - |R_n(\omega)|^2)}{\exp(-\Delta S_{BH}) \pm 1}, \quad (2.21)$$

$$-\frac{dQ}{dt} = \int_m^\infty \frac{d\omega}{2\pi} \sum_{\text{mods } n, \text{ charge } q} \frac{q(1 - |R_n(\omega)|^2)}{\exp(-\Delta S_{BH}) \pm 1}. \quad (2.22)$$

$S_{BH}$ , is the entropy of the black hole and  $\Delta S_{BH}$  is change of the entropy of black hole before and after radiation of the quanta of energy and charge,

$$\Delta S_{BH} = S(M - \omega, Q - q) - S(M, Q), \quad (2.23)$$

If  $A$  stands for the surface area of the black hole (area of the event horizon), then the black hole entropy, is given by Bekenstein-Hawking Formula,

$$S_{BH} = \frac{1}{4}A = \pi r_+^2 \left(1 - \frac{r_-}{r_+}\right)^{\frac{2\alpha^2}{1+\alpha^2}}. \quad (2.24)$$

The first law of black hole thermodynamics [1, 7] states,

$$dM = T_H dS_{BH} + \Phi_H dQ. \quad (2.25)$$

In the above formulae  $R_n(\omega)$ , is the reflection coefficient of emitted particle which can be obtained from the solution of wave equation with appropriate boundary condition.  $n$  is the angular parameters of the emitted particle that in this paper is replaced by  $\kappa$ , for spinors and  $l$ , for scalars.  $m$ ,  $\omega$  and  $q$ , are rest mass, energy and charge of the emitted particle. As we will see in the next section the equation take a simple form in tortoise coordinates defined as  $r_* = \int dr/f(r)^2$ . This coordinate maps the location of event horizon  $r = r_+$ , to  $r_* = -\infty$ . In this coordinate the boundary conditions or asymptotic behavior of the wave functions for the particles leaving the black hole horizon in terms of the transition and reflection coefficients are,

$$\Psi = \begin{cases} e^{+i(\omega - \frac{qQ}{r_+})r_*} + R_n(\omega)e^{-i(\omega - \frac{qQ}{r_+})r_*} & r \rightarrow r_+ \\ T_n(\omega)e^{+i\omega r} & r \rightarrow +\infty \end{cases}, \quad (2.26)$$

where  $\Psi$ 's are the asymptotic solutions of wave equations for outgoing modes.

The greybody factor defined as transition probability of wave in a given mode through the black hole potential, can be written in terms of the reflection coefficient as follows,

$$\gamma_n(\omega) = 1 - |R_n(\omega)|^2. \quad (2.27)$$

If we suppose the particles are coming from infinity into the black hole, these factors will indicate absorption coefficients of black hole. So, the greybody factors can be computed by obtaining the scattering coefficients of black hole. In the next section we will solve the corresponding equations to find these coefficients.

### 3. Charged massive Dirac particle in the background metric

In this section we address the main technical question of this article, emission of charged massive spin 1/2 particle in the background of dilaton black hole which is the key to our further analysis. Details of this calculation is presented in the appendix.

The equation of motion for spin 1/2 particle with charge  $q$  and mass  $m$  in the background metric (2.6) is;

$$(i\gamma^\mu D_\mu - m)\Psi = 0, \quad (3.1)$$

where

$$D_\mu = \partial_\mu + \Gamma_\mu - iqA_\mu, \quad (3.2)$$

$\Gamma_\mu$  is the spin connection defined by

$$\Gamma_\mu = \frac{1}{8} [\gamma^a, \gamma^b] e_a^\nu e_{b\nu;\mu}, \quad (3.3)$$

$e_\mu^a$ , the tetrad (vierbein) is

$$e_\mu^a = \text{diag} (f(r), f(r)^{-1}, R(r), R(r) \sin \theta). \quad (3.4)$$

We solve (3.1) by separation of variables and taking  $\Psi = f(r)^{-\frac{1}{2}} (\sin \theta)^{-\frac{1}{2}} \Phi$  [20, 36].

Let us define the operator  $K$

$$K = \gamma^t \gamma^r \gamma^\theta \frac{\partial}{\partial \theta} + \gamma^t \gamma^r \gamma^\varphi \frac{1}{\sin \theta} \frac{\partial}{\partial \varphi}. \quad (3.5)$$

with eigenvalues

$$\kappa = \begin{cases} (j + \frac{1}{2}) & j = l + \frac{1}{2}, \\ -(j + \frac{1}{2}) & j = l - \frac{1}{2}. \end{cases} \quad (3.6)$$

Here  $\kappa$  is a positive or negative integer ( $\kappa = \kappa_{(\pm)} = \pm 1, \pm 2, \dots$ ). Positive integers indicate (+) modes while negative integers indicate (−) modes.

One can show that after separation of radial and angular variables  $\Phi$  can be taken as;

$$\Phi = \begin{pmatrix} \frac{iG^{(\pm)}(r)}{R(r)} \phi_{jm}^{(\pm)}(\theta, \varphi) \\ \frac{F^{(\pm)}(r)}{R(r)} \phi_{jm}^{(\mp)}(\theta, \varphi) \end{pmatrix} e^{-i\omega t}, \quad (3.7)$$

with

$$\phi_{jm}^+ = \begin{pmatrix} \sqrt{\frac{l+1/2+m}{2l+1}} Y_l^{m-1/2} \\ \sqrt{\frac{l+1/2-m}{2l+1}} Y_l^{m+1/2} \end{pmatrix}, \quad (3.8)$$



for  $j = l + 1/2$   
and

$$\phi_{jm}^- = \begin{pmatrix} \sqrt{\frac{l+1/2-m}{2l+1}} Y_l^{m-1/2} \\ -\sqrt{\frac{l+1/2+m}{2l+1}} Y_l^{m+1/2} \end{pmatrix}. \quad (3.9)$$

for  $j = l - 1/2$

In this derivation we have followed [20–23, 28, 30, 36–38].

Defining  $F^{(\pm)}$  and  $\hat{G}^{(\pm)}$  by

$$\begin{pmatrix} \hat{F}^{(\pm)} \\ \hat{G}^{(\pm)} \end{pmatrix} = \begin{pmatrix} \sin(\theta_{(\pm)}/2) & \cos(\theta_{(\pm)}/2) \\ \cos(\theta_{(\pm)}/2) & -\sin(\theta_{(\pm)}/2) \end{pmatrix} \begin{pmatrix} F^{(\pm)} \\ G^{(\pm)} \end{pmatrix}, \quad (3.10)$$

with  $\theta_{(\pm)} = \text{arccot}(\kappa_{(\pm)}/mR(r))$ ,  $0 \leq \theta_{(\pm)} \leq \pi$  and the tortoise coordinate change  $r_* = \int f(r)^{-2} dr$ , we can separate equations to get,  $W_{(\pm)}$  and  $V_{(\pm)1,2}$ . Eventually, as shown in the appendix, the wave equations for spinors are ,

$$-\frac{\partial^2 \hat{F}}{\partial \hat{r}_*^2} + (V_1 - \omega^2) \hat{F} = 0. \quad (3.11)$$

$$-\frac{\partial^2 \hat{G}}{\partial \hat{r}_*^2} + (V_2 - \omega^2) \hat{G} = 0. \quad (3.12)$$

The radial potentials are

$$V_{1,2} = W^2 \pm \frac{\partial W}{\partial \hat{r}_*}, \quad (3.13)$$

$\hat{r}_*$  is the *generalized tortoise coordinate*,

$$\hat{r}_* = \int \frac{1}{f(r)^2} \left( 1 - \frac{qQ}{\omega r} + \frac{1}{2} f(r)^2 \frac{\frac{m}{\omega} \kappa}{(\kappa^2 + m^2 R(r)^2)} \frac{\partial R(r)}{\partial r} \right) dr, \quad (3.14)$$

and

$$W = f(r) \left( m^2 + \frac{\kappa^2}{R(r)^2} \right)^{\frac{1}{2}} \left( 1 - \frac{qQ}{\omega r} + \frac{1}{2} f(r)^2 \frac{\frac{m}{\omega} \kappa}{(\kappa^2 + m^2 R(r)^2)} \frac{\partial R(r)}{\partial r} \right)^{-1}. \quad (3.15)$$

The effective potential of scalars  $V_\eta$  and fermions  $V_{1,2}$  and also superpotential  $W^2$  have the common factor  $(1 - \frac{r_+}{r})(1 - \frac{r_-}{r})^{\frac{1-3\alpha^2}{1+\alpha^2}} \frac{1}{r^2}$  which approximately determines their main characteristics; the location of the maximum, its height, the behaviour at infinity and at the event horizon, for different charges and coupling constants. This factor shows that for  $\alpha = 1/\sqrt{3}$ , there is a turning point so that for this value the potential becomes independent of the charge. Note that since  $\frac{r_-}{r_+} = (1 + \alpha^2) \frac{Q^2}{r_+^2}$ , when  $r_+$  is kept constant  $\frac{r_-}{r_+}$  or effectively  $r_-$  represents the square of the charge. So when  $\alpha$  changes it passes through the turning point as a special point discussed more in the following.

The maximum of effective potential for both scalars and fermions is approximately,

$$\frac{r_{max}}{r_+} = 1 - \frac{1}{4} \left( \frac{3 - \alpha^2}{1 + \alpha^2} \epsilon - 2 \frac{1 - \alpha^2}{1 + \alpha^2} \right) + \frac{1}{4} \left( \left( \frac{3 - \alpha^2}{1 + \alpha^2} \epsilon - 2 \frac{1 - \alpha^2}{1 + \alpha^2} \right)^2 + 8\epsilon \right)^{\frac{1}{2}}, \quad (3.16)$$

where we have  $\epsilon = 1 - \frac{r_-}{r_+}$ .

For neutral black holes ( $\epsilon = 1$ ) the location of maximum is at  $r_{max} = \frac{3}{2}r_+$ . By gradually increasing the charge, the position of the maximum changes. The direction of its change depends on the value of coupling constant. When  $0 \leq \alpha < 1/\sqrt{3}$ , addition of charge, either positive or negative, pushes the position of the maximum away from the horizon which tends to  $r_{max} \rightarrow \frac{2r_+}{1+\alpha^2}$  at extremal limit when  $\epsilon$  goes to zero. In the case of  $\alpha = 1/\sqrt{3}$  the location of maximum doesn't change by change of black hole charge and is always in constant location  $r_{max} = \frac{3}{2}r_+$ . In the case  $1/\sqrt{3} < \alpha < 1$ , by increase of the charge, the location of maximum decreases and approaching extremality it tends to  $r_{max} \rightarrow \frac{2r_+}{1+\alpha^2}$ . In the case of  $\alpha \geq 1$ , when  $r_-$  approaches the extremal limit ( $\epsilon \rightarrow 0$ ), the position of the maximum moves toward the event horizon ( $r_{max} \rightarrow r_+$ ). In the case of  $\alpha \rightarrow \infty$  the maximum point approaches to  $r_{max} = (1 + \frac{\epsilon}{2})r_+$ . Hence the maximum is always in following ranges

$$\begin{cases} \frac{3}{2}r_+ \leq r_{max} \leq \frac{2}{1+\alpha^2}r_+ & 0 \leq \alpha < 1/\sqrt{3}, \\ \frac{2}{1+\alpha^2}r_+ \leq r_{max} \leq \frac{3}{2}r_+ & 1/\sqrt{3} \leq \alpha < 1, \\ r_+ \leq r_{max} \leq \frac{3}{2}r_+ & \alpha \geq 1. \end{cases} \quad (3.17)$$

Since  $V_1$  and  $V_2$  are supersymmetric partner potentials, they must have same spectra and maximum height [22].

Suppose  $\hat{r}_{*max}$  and  $\hat{r}_{*max1,2}$  are maximum of  $W$  and  $V_{1,2}$  in generalized tortoise coordinate respectively. We will conclude  $\hat{r}_{*max1} < \hat{r}_{*max} < \hat{r}_{*max2}$ . The zeros of the first derivative of effective potentials ( $\frac{\partial V_{1,2}}{\partial \hat{r}_*} = 2W \frac{\partial W}{\partial \hat{r}_*} \pm \frac{\partial^2 W}{\partial \hat{r}_*^2} = 0$ ) gives  $\hat{r}_{*max1,2}$ . In order to obtain  $\hat{r}_{*max1,2} = \hat{r}_{*max} + \Delta \hat{r}_{*max1,2}$  we expand  $\frac{\partial V_{1,2}}{\partial \hat{r}_*} = 0$  around  $\hat{r}_{*max}$ . This gives,

$$\begin{cases} \Delta \hat{r}_{*max1} = -1 \left/ \left[ 2W + \frac{\partial}{\partial \hat{r}_*} \ln \left( \frac{\partial^2 W}{\partial \hat{r}_*^2} \right) \right] \right|_{\hat{r}_{*max}}, \\ \Delta \hat{r}_{*max2} = 1 \left/ \left[ 2W - \frac{\partial}{\partial \hat{r}_*} \ln \left( \frac{\partial^2 W}{\partial \hat{r}_*^2} \right) \right] \right|_{\hat{r}_{*max}}. \end{cases} \quad (3.18)$$

To conclude that  $\hat{r}_{*max1} < \hat{r}_{*max} < \hat{r}_{*max2}$  we shall show that the denominators of the above equations are allways positive. With this aim we calculate  $\frac{\partial^2 V_{1,2}}{\partial \hat{r}_*^2}$  at  $\hat{r}_* = \hat{r}_{*max}$ .

$$\frac{\frac{\partial^2 V_{1,2}}{\partial \hat{r}_*^2} \Big|_{\hat{r}_{*max}}}{\frac{\partial^2 W}{\partial \hat{r}_*^2} \Big|_{\hat{r}_{*max}}} = \left[ 2W \pm \frac{\partial}{\partial \hat{r}_*} \ln \left( \frac{\partial^2 W}{\partial \hat{r}_*^2} \right) \right]_{\hat{r}_{*max}} \quad (3.19)$$

Owing to similar behavior of supersymmetric partner potentials  $V_{1,2}$  (Figure 1) and their superpotential  $W$ , sign of their concavity (which is negative) must be

equal. Consequently, above expression is always positive. Furthermore, as we have  $\Delta \hat{r}_{*max1,2} \simeq \frac{\Delta r_{max1,2}}{f(r_{max})^2}$  from (3.14), it leads to  $r_{max1} < r_{max} < r_{max2}$ .

As shown before the peak of  $V_1$  is closer to the horizon, so for better approximation we analyse  $V_1$ . Suppose we are near extremal condition, we distinguish three different behaviour for the  $r_{max}$ .

For  $\alpha < 1$  we have  $r_{max} \rightarrow \frac{2}{1+\alpha^2}r_+$ , and for  $\alpha = 1$ ,  $r_{max} \rightarrow (1 + \sqrt{\frac{\epsilon}{2}})r_+$  and in the case of  $\alpha > 1$  we obtain  $r_{max} \rightarrow \left(1 + \frac{1}{2} \frac{\alpha^2+1}{\alpha^2-1} \epsilon\right) r_+$ .

For fermions the value of the maximum approximately is

$$(V_{1,2})_{max} \simeq \left(\frac{1+\alpha^2}{2r_+}\right)^2 \frac{\kappa \left(\kappa + \frac{1-\alpha^2}{2}\right)}{\left(1 - \frac{qQ}{\omega r_+}\right)^2 \left(\frac{1-\alpha^2}{2}\right)^{\frac{2\alpha^2-2}{\alpha^2+1}}}, \quad \alpha < 1, \quad (3.20)$$

and

$$(V_{1,2})_{max} \simeq \frac{\kappa^2}{r_+^2 \left(1 - \frac{qQ}{\omega r_+}\right)^2}, \quad \alpha = 1, \quad (3.21)$$

and

$$(V_{1,2})_{max} \simeq \frac{\kappa \left(\kappa + \frac{1-\alpha^2}{1+\alpha^2}\right)}{r_+^2 \left(1 - \frac{qQ}{\omega r_+}\right)^2 \left[\frac{1}{2} \frac{\alpha^2-1}{\alpha^2+1} \left(1 - \frac{r_-}{r_+}\right)\right]^{\frac{2\alpha^2-2}{\alpha^2+1}}}, \quad \alpha > 1, \quad (3.22)$$

For scalars the height of the maximum can be approximately obtained from (2.16) as follows

$$(V_\eta)_{max} \simeq \left(\frac{1+\alpha^2}{2r_+}\right)^2 \frac{\left((l + \frac{1}{2})^2 + \frac{1}{4}(1-\alpha^2)\right)}{\left(\frac{1-\alpha^2}{2}\right)^{\frac{2\alpha^2-2}{1+\alpha^2}}}, \quad \alpha < 1, \quad (3.23)$$

and

$$(V_\eta)_{max} \simeq \frac{(l + \frac{1}{2})^2}{r_+^2}, \quad \alpha = 1, \quad (3.24)$$

and

$$(V_\eta)_{max} \simeq \frac{(l + \frac{1}{2})^2 - \frac{1}{4} \left(\frac{1-\alpha^2}{1+\alpha^2}\right)^2}{r_+^2 \left[\frac{1}{2} \frac{\alpha^2-1}{\alpha^2+1} \left(1 - \frac{r_-}{r_+}\right)\right]^{\frac{2\alpha^2-2}{\alpha^2+1}}}, \quad \alpha > 1. \quad (3.25)$$

In the case of neutral black holes ( $r_{max} \rightarrow \frac{3}{2}r_+$ ) the maximums for fermions and scalars are

$$(V_{1,2})_{max} \simeq \frac{4}{27} \frac{\kappa^2}{r_+^2}, \quad (3.26)$$

$$(V_\eta)_{max} \simeq \frac{4}{27} \frac{l(l+1) + \frac{2}{3}}{r_+^2}. \quad (3.27)$$

Figure 1 shows plots of potential for fermions for different values of  $\alpha$  and black hole charge, from which one can observe the behavior discussed above.

Comparing the maximum of the potentials for scalars and fermions from previous equations and figures 2a and 2b we see that the value for the scalars is always less than that of fermions. Consequently, the greybody factors for scalars (figure 2c) would be greater than that of fermions (figure 2d). Besides, as scalars obey Bose-Einstein statistics in thermal emission they would provide a much larger share of the black hole energy emission with respect to fermions (figure 2e and 2f). Note that the charge of the emitted particle appears as the product  $qQ$  in the denominators of  $W$  and in the maximum of the potential (3.22). The maximum is higher for the case when the emitted charge has the same sign as the black hole. Surprisingly emission of the opposite charge is easier. We shall see this effect quantitatively when we calculate the greybody factors. When  $q = 0$ , we obtain the result for the emission of uncharged fermions such as neutrinos. In this case only the gravitational force acts on the particle. Also, it can be seen that the metric factor at the horizon is zero  $f(r_+)^2 = 0$ , where the potential also vanishes. At infinity  $W^2$  and the potential will be equal to  $m^2$ . The expression for superpotential  $W^2$  shows there is an angular term  $\frac{\kappa^2}{R(r)^2}$  which vanishes at the extremal limit. The same factor decreases as  $\alpha$  increases. Therefore, the height of potential barrier increases as the value of coupling constant increases indicating that the coupling constant can have significant effect on greybody factors and evaporation rates of the black hole.

The potential barrier grows as the second power of the angular variable  $\kappa$  as a result of which we expect lower emission of higher angular momenta. The angular momentum term  $\frac{\kappa^2}{R(r)^2}$  is very distinct for the dilaton black hole and approaches  $\frac{\kappa^2}{r^2}$  for the normal black hole. At the extremal limit where  $r_- \rightarrow r_+$ , this term  $\frac{\kappa^2}{R(r)^2}$  diverges. But the maximum value of the potential (3.20) for  $\alpha < 1$  remains finite although small, and for  $\alpha > 1$ , (3.22) becomes very large and divergent.

At  $\alpha = 1$  the maximum (3.21) remains finite.

#### 4. Greybody factors and dilaton black hole evolution

In this section we find the greybody factors which are essential in the evolution of the black hole. The backreaction which also heavily modifies both elements is taken into account. The greybody factors are calculated with analytical approximation and also numerical method. Although our conclusions rely upon the numerical computations, the analytical approximation gives insight to the results obtained.

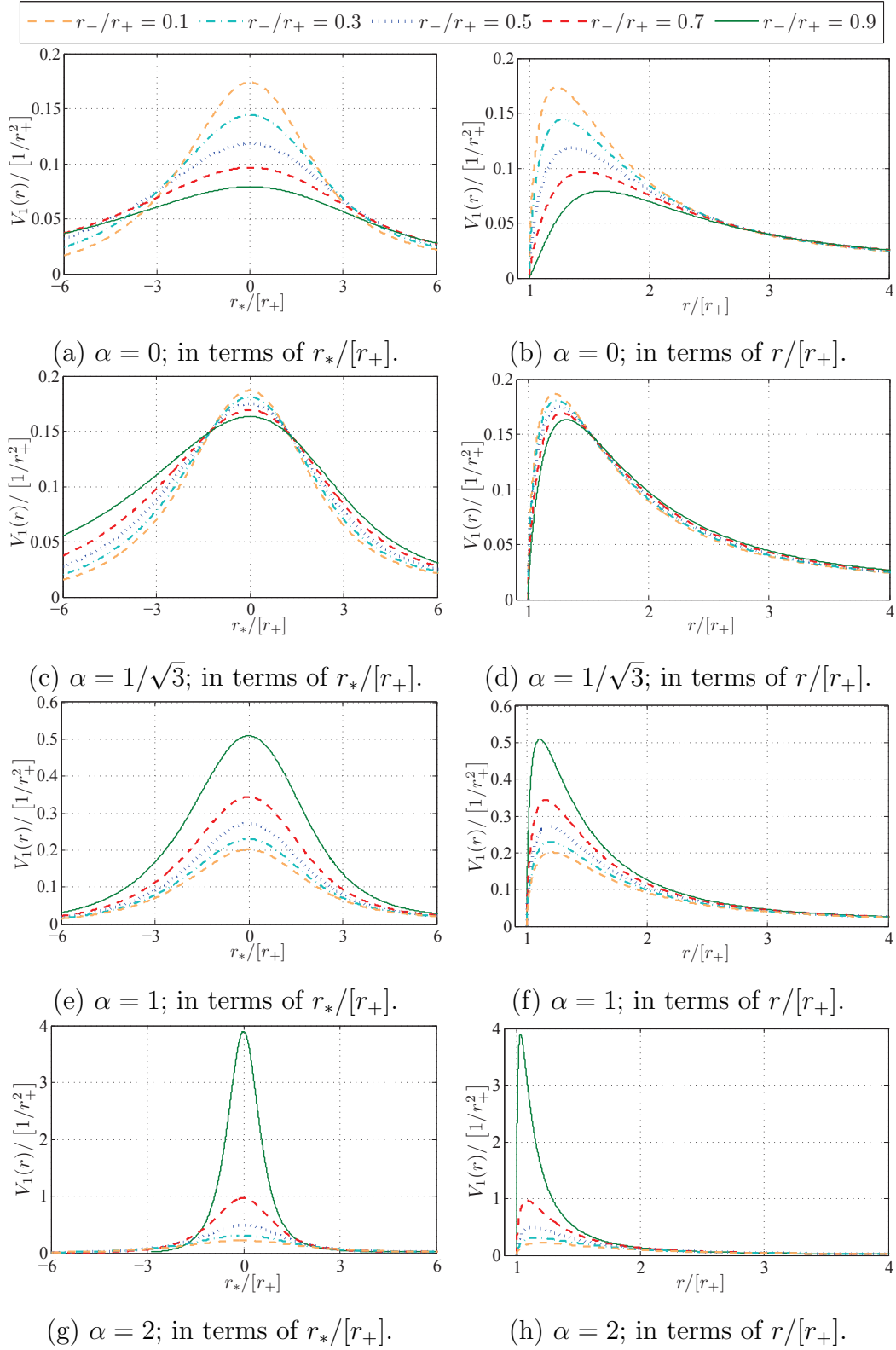


Figure 1: Plots of potential for black holes with  $\alpha = 0, 1/\sqrt{3}, 1, 2$  and different values of charge ( $r_-/r_+ = (1 + \alpha^2) \frac{Q^2}{r_+} = 0.1, \dots, 0.9$ ) in natural units and numerical values  $G = \hbar = c = 4\pi\epsilon_0 = 1$ ,  $r_+ = 100$ . Spin  $\frac{1}{2}$  particles with  $\kappa = 1$ .

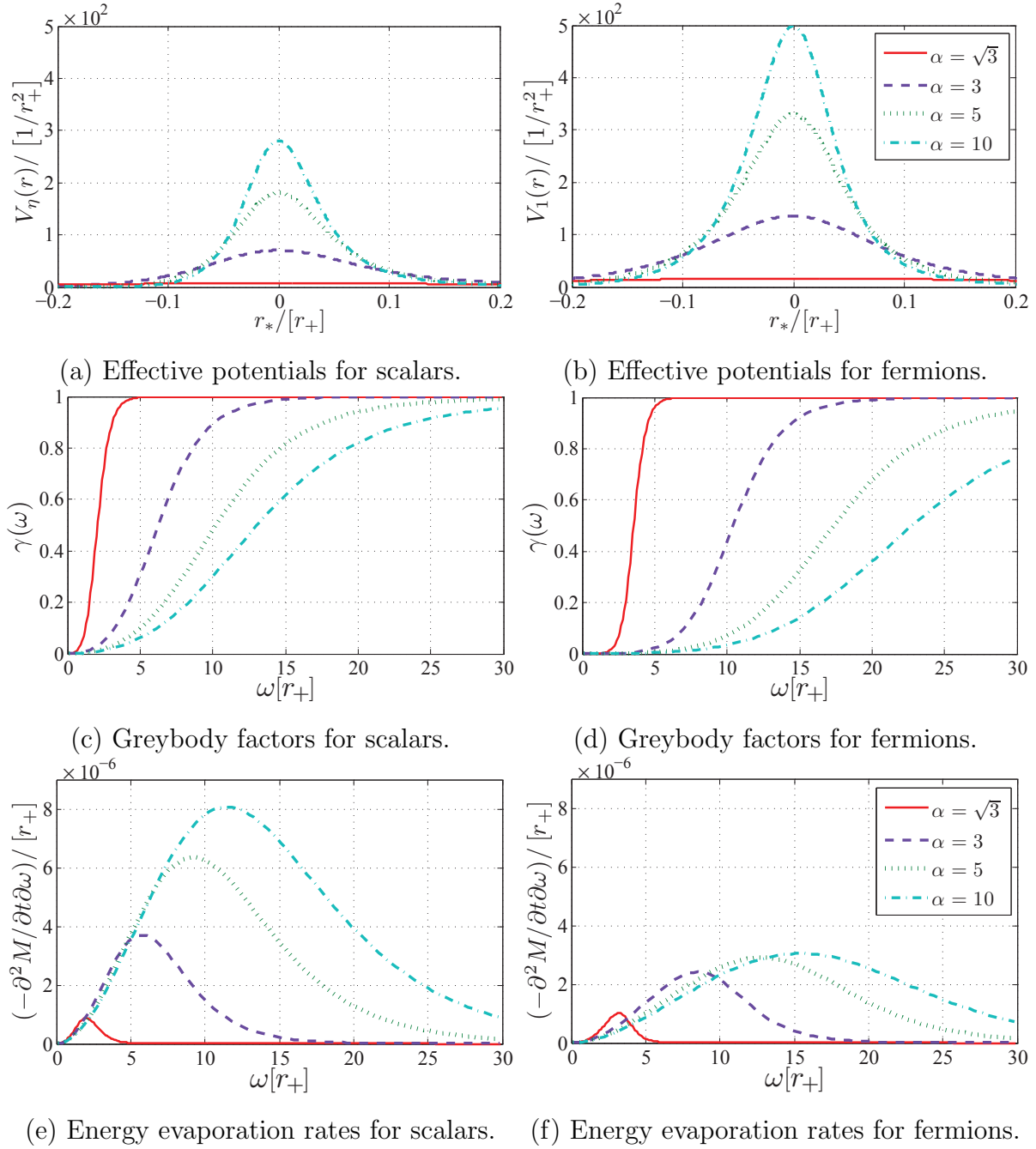


Figure 2: Comparison of dominant mode ( $l = 0, \kappa = 1$ ) of potentials, greybody factors and energy evaporation rates of scalars with fermions for different values of  $\alpha$  in natural units and numerical values  $G = \hbar = c = 4\pi\epsilon_0 = 1$ ,  $r_-/r_+ = 0.98$ ,  $r_+ = 100$ .

#### 4.1. Inclusion of backreaction correction

As stated previously the temperature of dilaton black holes plays a significant role on their behavior. The temperature at the extremal limit vanishes for  $\alpha < 1$ , tends to  $\frac{1}{4\pi r_+}$  for  $\alpha = 1$  and diverges for  $\alpha > 1$ . For  $\alpha < 1$  as approaching the extremal limit the temperature tends to zero and the black hole cools. While for  $\alpha > 1$  the divergence of the temperature seems to lead to the eruption of the black hole. On the other hand, in this case the inclusion of backreaction will show that the geometry outside the event horizon prevents the decay of the black hole and cools off its radiation completely at the extremal limit. Thanks to this correction the solution provides a more dynamical picture. In this part first we will explain the inclusion of this correction into the solution and then try to show the effect of this correction by analytical approach, for a better clarification of the situation. Due to similarity between equations of scalars and fermions analytical solution is provided only for fermions. Finally the inclusion of this correction which is more evident in high frequency are presented in figures 4b, 7a, 7d, 10 with numerical solution. The  $\alpha = 1$  case needs higher order corrections which is delegated to the future works.

Indeed, emission of a quanta of energy  $\omega$  and charge  $q$  changes the mass  $M$  and charge  $Q$  of the black hole. Hence, to the first order of backreaction correction one can subtract the lost energy and charge from the black hole and solve the equations in the new background geometry. With this aim we insert  $\dot{M} = M - \omega$  and  $\dot{Q} = Q - q$  into all the equations. In this way we resort to an adiabatic approximation and use the formulae (2.21) and (2.22) at every step of the evolution of the black hole.

According to (3.22) for fermions and (3.25) for scalars in  $\alpha > 1$  the maximum of the effective potentials grows as the black hole approaches the extremal limit, where it diverges. Consequently, the emitted particle carrying an amount of energy and charge of the black hole pushes it toward the extremal limit or  $\frac{r'_-}{r_+} > \frac{r_-}{r_+}$ . This causes the potential barrier to grow and prevent the process.

As was obtained previously the place of the maximum of the effective potential, for both fermions and scalars, approaches the event horizon as the black hole approaches the extremal limit,  $r_+ \rightarrow \left(1 + \frac{1}{2} \frac{\alpha^2 + 1}{\alpha^2 - 1}\right)$ . In the analytical solution of wave equation at the extremal limit we need the solution of generalized tortoise coordinate (3.14) near the event horizon. In this limit given  $\frac{qQ}{\omega r_+} \simeq \frac{q}{\omega \sqrt{1 + \alpha^2}}$  assuming  $Q > 0$  we have,

$$\hat{r}_*|_{r_+ \simeq r_-, r \simeq r_+} \simeq \int_r \frac{\left(1 - \frac{q}{\omega \sqrt{1 + \alpha^2}}\right)}{\left(1 - \frac{r_+}{r}\right)^{\frac{2}{1 + \alpha^2}}} dr \bigg|_{r \simeq r_+} \simeq \frac{\alpha^2 + 1}{\alpha^2 - 1} r_+^{\frac{2}{\alpha^2 + 1}} \left(1 - \frac{q}{\omega \sqrt{1 + \alpha^2}}\right) (r - r_+)^{\frac{\alpha^2 - 1}{\alpha^2 + 1}}, \quad (4.1)$$

Contrary to the expectations, this tortoise coordinate at the extremal limit and for  $\alpha > 1$  at the limit  $r \rightarrow r_+$  is finite, while in other cases it tends to  $-\infty$ . This can be observed in figure 1g where the width of the potential barrier decreases as the black

hole approaches the extremal limit.

In order to obtain the magnitude of the influence of the backreaction on the high frequency results, we first need to calculate the change in the potential barrier under the emission of quantum of energy  $\omega = -\delta M$  and charge  $q = -\delta Q$ , respectively the changes in mass and charge of the of black hole. We have used the maximum height of the potential barrier obtained in (3.22) on the grounds that it can be approximated with potential barrier near the event horizon. Then, the effect reflected on the in inner ( $r'_- = r_- + \delta r_-$ ) and outer ( $r'_+ = r_+ + \delta r_+$ ) horizon assuming near extremal limit ( $Q = \sqrt{1 + \alpha^2}M$ ,  $r_+ \simeq r_- \simeq (1 + \alpha^2)M$ ) are calculated,

$$\begin{cases} \delta r_+ = \left(1 + \frac{1}{\alpha^2}\right) \delta M + \frac{(\alpha^2-1)(\alpha^2+1)^{1/2}}{\alpha^2} \delta Q, \\ \delta r_- = -\left(1 + \frac{1}{\alpha^2}\right) \delta M + \frac{(\alpha^2+1)^{3/2}}{\alpha^2} \delta Q. \end{cases} \quad (4.2)$$

For the case  $\alpha > 1$  the denominator of (3.22), where the term  $1 - \frac{r_-}{r_+}$  causes the effective potential to diverge at the extremal limit, plays a significant role on the black hole behaviour when backreaction correction is applied. The change of this term under the change of black hole mass  $\delta M$  and charge  $\delta Q$  is ,

$$1 - \frac{r'_-}{r'_+} = \epsilon + \frac{2}{\alpha^2} \left( \frac{\delta M}{M} - \frac{\delta Q}{Q} \right). \quad (4.3)$$

where we have  $\epsilon = 1 - \frac{r_-}{r_+}$ .

Suppose under the emission of the quantum of energy  $\omega = -\delta M$  and charge  $q = -\delta Q$  this term vanishes. Consequently, the effective potential diverges and as a result the passage of the particle through the potential barrier is impeded. Hence,  $1 - \frac{r'_-}{r'_+} = 0$  puts an upper limit on the high cutoff frequency ( $\omega_{HCF}$ ).

$$\omega_{HCF} = \frac{\alpha^2}{2} M \epsilon + \frac{q}{\sqrt{1 + \alpha^2}}. \quad (4.4)$$

Of course as we will discuss below the true high frequency cut off is much smaller.

As the black hole approaches the extremal limit ( $\epsilon \rightarrow 0$ ), this high cutoff frequency tending to  $\omega_{HCF} \rightarrow \frac{q}{\sqrt{1 + \alpha^2}}$  decreases. Obviously, because of the emission of other neutral particles with zero second term ( $\frac{q}{\sqrt{1 + \alpha^2}} = 0$ ) and opposite sign charged particles, this high cutoff frequency would be smaller than the obtained value. In addition, as can be observed from figure 10a, as the black hole approaches the extremal limit the low cutoff frequency  $\omega_{LCF}$ , specified by the greybody factor, increases as a function of temperature of black hole ( $\omega_{LCF} \propto T_H$ ) divergent in this limit. Hence in this limit the Hawking radiation of the black hole would be strongly suppressed.

After the emission of particle from event horizon, the maximum of the potential (3.22) changes,  $(V'_{1,2})_{max} = (V_{1,2})_{max} + \delta(V_{1,2})_{max}$ . In this limit given  $\frac{qQ}{\omega r_+} \simeq \frac{q}{\omega \sqrt{1 + \alpha^2}}$  we



have,

$$(\dot{V}_{1,2})_{max} \simeq \frac{\kappa \left( \kappa + \frac{1-\alpha^2}{1+\alpha^2} \right)}{r_+^2 \left( 1 - \frac{q}{\omega\sqrt{1+\alpha^2}} \right)^2 \left[ \frac{1}{2} \frac{\alpha^2-1}{\alpha^2+1} \left( \epsilon - \frac{2}{\alpha^2} \left( \frac{\omega}{M} - \frac{q}{Q} \right) \right) \right]^{\frac{2\alpha^2-2}{\alpha^2+1}}}, \quad (4.5)$$

This equation shows as the black hole emits particle with  $\omega > \frac{M}{Q}q$ , the height of potential barrier grows and it reduces the greybody factors.

In order to obtain the change in the greybody factors  $\dot{\gamma}(\omega)$  after inclusion of backreaction correction, we approximate the change of the maximum of the potential barrier  $\delta(V_{1,2})_{max}$  to the first order under this correction,

$$\delta(V_{1,2})_{max} \simeq \frac{4}{\alpha^2\epsilon} \frac{\alpha^2-1}{\alpha^2+1} \left( \frac{\omega}{M} - \frac{q}{Q} \right) (V_{1,2})_{max}. \quad (4.6)$$

To obtain the greybody factors WKB approximation is used. This approximation gives the transmission probability from a potential well [22]. However, because the change of the greybody factors is needed only and the peak of the potential barrier is near the horizon, we separate the  $\delta(V_{1,2})_{max}$  part and integrate over this near the event horizon and obtain,

$$\begin{aligned} \dot{\gamma}(\omega) &\simeq \exp \left( -2 \int \sqrt{V_{1,2}(r) + \delta V_{1,2}(r) - \omega^2} d\hat{r}_* \right) \\ &\simeq \gamma(\omega) \exp \left( -2 \int \frac{1}{2} \frac{\delta V_{1,2}(r)}{V_{1,2}(r) - \omega^2} d\hat{r}_* \right) \\ &\simeq \gamma(\omega) \exp \left( - \int_{r \simeq r_+}^{(1 + \frac{\alpha^2+1}{\alpha^2-1}\epsilon)r_+} \frac{\delta(V_{1,2})_{max}}{(V_{1,2} - \omega^2)_{max}} d\hat{r}_* \right). \end{aligned} \quad (4.7)$$

where  $\gamma(\omega)$  is greybody factors without the backreaction correction. On the grounds that maximum height of potential at the extremal limit is near the event horizon ( $r_{max} \simeq \left( 1 + \frac{1}{2} \frac{\alpha^2+1}{\alpha^2-1} \epsilon \right) r_+$ ), the integral is taken over  $r \simeq \left[ r_+, \left( 1 + \frac{\alpha^2+1}{\alpha^2-1} \epsilon \right) r_+ \right]$  region. In this range of integration we can assume  $\delta(V_{1,2})_{max}$  be a constant. Finally, the greybody factors under the inclusion of backreaction is given by,

$$\dot{\gamma}(\omega) \simeq \gamma(\omega) \exp \left( - \frac{4\omega}{\epsilon} \left( 1 + \frac{1}{\alpha^2} \right) \left( 1 - \frac{q}{\omega\sqrt{1+\alpha^2}} \right)^2 \left( \frac{\alpha^2+1}{\alpha^2-1} \epsilon \right)^{\frac{\alpha^2-1}{\alpha^2+1}} \right). \quad (4.8)$$

Note that here we have assumed that the charge of black hole is positive ( $\frac{qM}{\omega Q} = \frac{q}{\omega\sqrt{1+\alpha^2}}$ ).

This expression shows that the backreaction correction always reduces the greybody factors. Moreover the term  $\left( 1 - \frac{q}{\omega\sqrt{1+\alpha^2}} \right)^2$  shows that the greybody factors at high frequency make the black hole to lose charge, as can be observed from figure 7d in high frequency. Besides, we obtain the important result in equation (4.8) which is also shown in figure 10a that as the black hole approaches the extremal limit  $\epsilon \rightarrow 0$  the greybody factors  $\dot{\gamma}(\omega)$  vanishes.

One may question the contributions that change of temperature due to backreaction will have on the emission rates and other quantities of interest. We draw the attention of the reader that this effect is already taken into account. We have used the formulae (2.21) and (2.22) for decay rates that are given in terms of  $\Delta S$  which include all changes as well as the change in the temperature. What is implicit in our approach is the use of  $r_+$ ,  $r_-$ , the radii of the outer and inner horizons and their changes to compute other quantities. The change in temperature can also be expressed in terms of  $\delta r_{\pm}$ , reflected in  $\Delta S$  used in (2.23) and the effective potentials (4.5) discussed. Hence one need not consider it separately.

#### 4.2. Analytical approximation and numerical solution

To calculate the greybody factors [9–17, 44] we need to solve (3.11) and (3.13). Analytical solutions to such equations are formidable. We choose two methods of approximations to solve these equations. First we approximate the potential by a solvable potential, the Rosen-Morse potential [39–41] and then we solve the equations numerically. Using this potential quasi-normal modes of several black holes have been obtained [37, 47–51]. The numerical solution helps us to estimate the errors of our analytical approach. As we shall see later the approximation is quite reliable.

We also include corrections due to the backreaction. This correction becomes important when the black hole approaches the extremal limit.

We use adiabatic approximation to include the effect of the emission of particles. Like previous works we assume the emission rate is not too large and hence at any moment the black hole configuration remains unchanged as (2.6) except that the mass and charge have changed,  $M \rightarrow M - \delta m$  and  $Q \rightarrow Q - \delta q$ . This enables us to use the rates calculated by taking  $M$  and  $Q$  constant. Obviously approaching the extremal limit without applying the correction the results are not as reliable.

Rosen-Morse potential, originally devised to investigate diatomic molecules has an attractive core approximating the vibrational states, but approaches a constant to allow dissociated states. In our case it is parameterized as [41]

$$V(\hat{r}_*) = \frac{V_{+\infty} + V_{-\infty}}{2} + \frac{V_{+\infty} - V_{-\infty}}{2} \tanh\left(\frac{\hat{r}_*}{\lambda}\right) + \frac{V_0}{\cosh^2(\hat{r}_*/\lambda)}. \quad (4.9)$$

To fix the parameters we match it with the black hole potential (3.13) at the boundaries  $r^* \rightarrow \pm\infty$

$$\begin{cases} V_{+\infty} = \lim_{\hat{r}_* \rightarrow +\infty} V_{1,2} = m^2, \\ V_{-\infty} = \lim_{\hat{r}_* \rightarrow -\infty} V_{1,2} = 0, \end{cases} \quad (4.10)$$

and its value at the maximum,

$$V_0 = \frac{1}{2}V_{max} - \frac{1}{4}m^2 + \frac{1}{2}\sqrt{V_{max}^2 - m^2V_{max}} \simeq V_{max}. \quad (4.11)$$

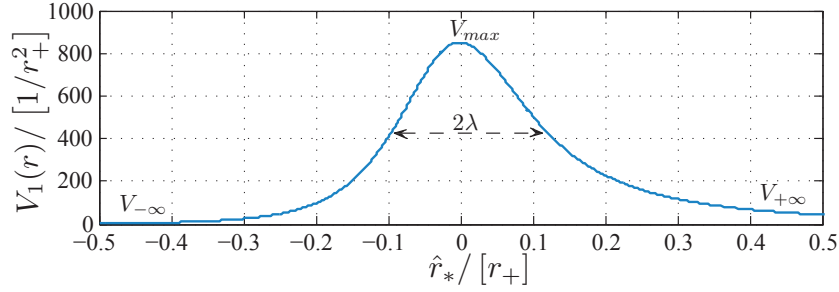


Figure 3: Plot of potential in terms of  $\hat{r}_*/[r_+]$ .  $V_{+\infty}$  and  $V_{-\infty}$  are black hole potential asymptotic values and  $V_{max}$  is its maximum value.

where  $V_{max}$  is maximum value of black hole potential. When  $\frac{m^2}{V_{max}} \ll 1$  it will become equal to  $V_0$ . In (4.9),  $\lambda$  indicates the width of black hole potential. An approximation in obtaining  $\lambda$  is finding the distance  $\hat{r}_{*\lambda}$  of maximum of black hole potential location from its half in tortoise coordinate,

$$\frac{V_{max}}{2} \simeq \frac{V_{max}}{\cosh^2(\hat{r}_{*\lambda}/\lambda)}, \quad (4.12)$$

In the above equation for simplicity the mass term is neglected. Hence,  $\lambda$  as a function of  $\hat{r}_{*\lambda}$  is given by,

$$\lambda \approx \frac{\hat{r}_{*\lambda}}{\ln(\sqrt{2} \pm 1)}. \quad (4.13)$$

These parameters are schematically shown in figure 3.

Solving the equations with Rosen-Morse potential replaced for the true black hole potential, one obtains the reflection coefficient and the greybody factors [41],

$$\gamma(\omega, \kappa) = \frac{\sinh(\pi\lambda\sqrt{\omega^2 - m^2}) \sinh(\pi\lambda\omega)}{\sinh^2(\pi\lambda(\omega + \sqrt{\omega^2 - m^2})/2) + \cosh^2(\pi\sqrt{\lambda^2 V_0 - 1/4})}. \quad (4.14)$$

The Rosen-Morse potential for our case is compared with numerical plot of potential (3.13) in figure 4a. As it can be seen the difference looks negligible. In figure 4b we will also compare the results of the greybody factors (obtained by the two methods). The relative error is less than 2%. The errors at the low frequency limit is larger than the errors in the high frequency limit. This make the low frequency errors more serious since they have stronger effect on the evaporation rates.

Although the numerical results are more reliable but the analytic results obtained by above approximation allows us to explore the behaviour of the greybody factors more intuitively.

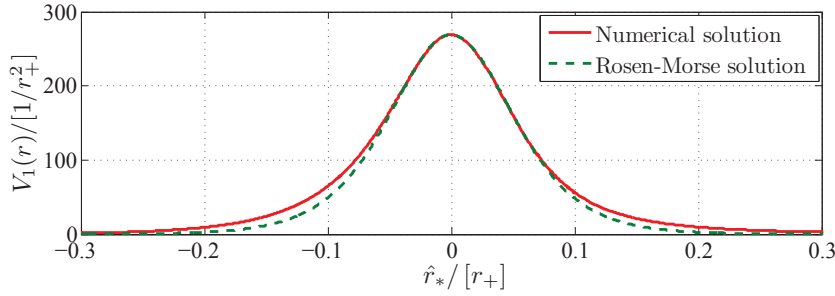
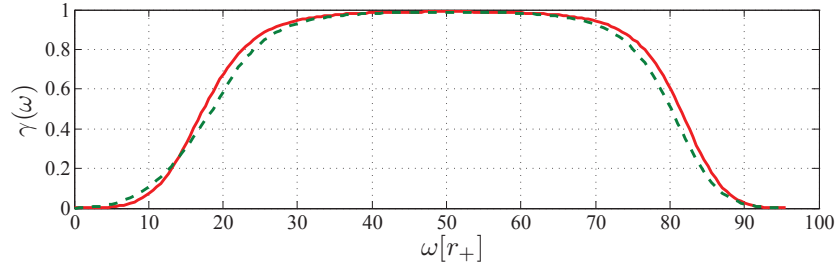
(a) Rosen-Morse potential and exact potential in terms of  $\hat{r}_*/[r_+]$ .(b) Greybody factors obtained by Rosen-Morse and numerical calculation in terms of frequency  $\omega[r_+]$ .

Figure 4: Black hole with parameters  $r_-/r_+ = 0.98$ ,  $\alpha = 5$  and particles with angular momentum  $\kappa = 1$ . Relative errors are almost 2%. Natural units and numerical values are  $G = \hbar = c = 4\pi\epsilon_0 = 1$  and  $r_+ = 100$ .

#### 4.3. Evolution and fate of the dilaton black hole

In this part we explore the evolution and fate of the dilaton black hole. We shall pay particular attention to the conditions under which the black hole evolves to two possible final states, spontaneously evaporating towards extremal limit, or complete evaporation. We call the boundary of the separation of these two conditions in the  $(Q/M, \alpha)$  plane (figure 5), the transition line. So we distinguish two regimes in this plane, a region of parameter where the final fate is an extremal black hole which we call "extremal regime" and a region in which the final condition is total evaporation called "decay regime". We have avoided to call these conditions "phase" since that will cause a misunderstanding with thermodynamical phases.

The existence of this transition line is easily shown by going to certain limits. First we prove that there is certain regions that the final fate of the black hole is inevitably extremal case. We show this for at least two regions of the parameters, for very large  $\alpha$  and the other when  $Q/M > q/m$ . First we discuss the case for large  $\alpha$ .

If we go to large  $\alpha$ , equation (2.20) shows that the positive and the negative charges are emitted with equal rate. To see this more carefully, note that in the charge flux both greybody factors and Boltzmann factor in Hawking radiation, depend on  $\frac{|qQ|}{\omega r_+}$ . Also note that when both sign of charge are emitted the charge evaporation reduces and it may hinder the motion of the black hole in the  $(Q/M, \alpha)$  plane away from the extremal

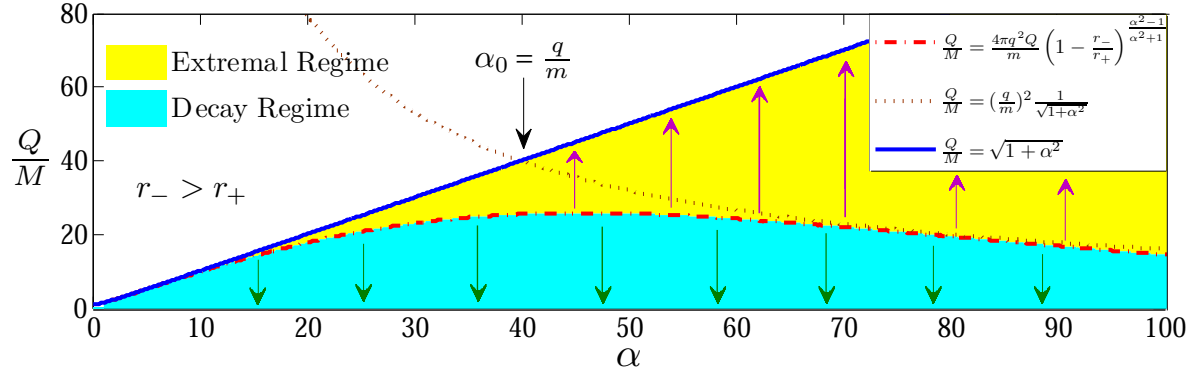


Figure 5: Plot of transition line, extremal line, extremal regime, decay regime, and direction of evolution and fate of dilaton black hole. Upward arrows in the extremal regime, show the direction of black hole evolution towards extremal limit (flat geometry for  $\alpha \gg 1$ ), downward arrows in the decay regime show its direction of evolution towards neutral black hole (Schwarzschild black hole) which finally leads to complete evaporation. Numerical values are  $\alpha_0 = 40$ ,  $mM = 1/2\pi$

line ( $\frac{Q}{M} = \sqrt{1 + \alpha^2}$ ). Since  $\frac{qQ}{\omega r_+} < \frac{q}{\omega \sqrt{1 + \alpha^2}}$ , we see that for large  $\alpha$ ,  $\frac{qQ}{\omega r_+} \rightarrow 0$ , and this causes the net charge emission rate to vanish. But meanwhile the energy keeps being radiated. Since for a fixed charge there is a lower limit for the mass of the black hole ( $M > Q/\sqrt{\alpha^2 + 1}$ ), finally the energy radiation must also come to halt resulting in an extremal state.

Before discussing the other case let us explore an illuminating property of the large  $\alpha$  case. When  $\alpha$  is much larger than 1, the geometry (2.6) becomes flat in the extremal black hole case. So any black hole geometry in this regions ( $\alpha$  large) and extremal regime (figure 5) taking  $r' = r - r_-$  will end up in an extremal state with a flat background geometry.

$$ds^2 = dt^2 - dr'^2 - r'^2 d\Omega^2. \quad (4.15)$$

Therefore it will look like an elementary particle [3] in a flat space.

Now let us turn to other example which will also help us to find a mathematical discipline of the line separating two regimes mentioned.

Another case where similar phenomena happens is where in the process of emission of charge and mass, the black hole moves close to the extremal limit. Since it emits both positive and negative charges  $\pm q$ , the effective charge emitted is a positive fraction of the same sign charge  $\xi q$  ( $0 \leq \xi < 1$ ). Then the effective charge  $q' = -\delta Q$  emitted per one quanta of mass  $m = -\delta M$ , is less than  $q$  the quantum of charge. So we define  $q'/q = \xi$  a ratio to be found. This parameter can be obtained from  $\frac{q}{m}\xi = \frac{dQ}{dM}$ , where  $dQ = \dot{Q} - Q$  and  $dM = \dot{M} - M$  are the change of black hole charge and mass during an infinitesimal radiation process and is a function of  $(\alpha, Q, M, \frac{q}{m})$ . Then if  $\dot{Q}/\dot{M}$  is larger than  $Q/M$ , the black hole has moved closer to the extremal limit, and when this process continues

finally it will end up with extremal parameters and the radiation stops. Such condition is satisfied if  $\frac{Q-\xi q}{M-m} > \frac{Q}{M}$  or equivalently considering the condition  $\frac{Q}{M} < \sqrt{\alpha^2 + 1}$ ;

$$\frac{\xi q}{m} < \frac{Q}{M} < \sqrt{\alpha^2 + 1}. \quad (4.16)$$

This completes the proof for the non-emptiness of the extremal regime. It covers a large area in the  $(Q/M, \alpha)$  plane as shown in figure 5.

To see that there are also black holes that evaporate completely we give two examples;

One is the case where  $\alpha = 0$  i.e. the RN black hole which is well known to lose charge very quickly and then totally evaporate [6, 8]. The other example when a black hole with a given  $Q/M$  moves away from the extremal condition after emission of charge  $\xi q$  and mass  $m$ . This means when  $\frac{Q}{M} < \xi \frac{q}{m}$ .

So we have proven the existence of the two regimes which must be separated with a transition line mathematically specified by  $\frac{Q}{M} = \xi \frac{q}{m}$  from the equation (4.16) and is plotted in figure 5.

Having the definition for the transition line ( $\frac{Q}{M} = \xi \frac{q}{m}$ ) we can proceed to calculate it.

Before performing any detailed calculation let us estimate the transition line for large  $\alpha$ . As discussed previously as  $\alpha$  increases charge flux decreases and tends to zero as  $\frac{q}{m} \frac{1}{\sqrt{\alpha^2 + 1}} \rightarrow 0$ , while the energy flux remains finite. Hence, at this limit  $\xi$  which is the ratio of charge flux to energy flux ( $\frac{q}{m} \xi = \frac{dQ}{dM}$ ) tends to zero. As we will show bellow  $\xi < \frac{q}{m} \frac{1}{\alpha^2 + 1} < 1$  (4.19), for small  $\frac{q}{m} \frac{1}{\sqrt{\alpha^2 + 1}}$ .

Also, the line  $\frac{Q}{M} = \frac{(q/m)^2}{\sqrt{\alpha^2 + 1}} = \frac{\alpha_0^2}{\sqrt{\alpha^2 + 1}}$  gives an upper limit approximation for the transition line which is shown in figure 5. This holds for  $\alpha > \alpha_0 (= \frac{q}{m})$  and  $T_H > m$ .

This line intersects the boundary line of  $r_- \leq r_+$  given by  $\frac{Q}{M} = \sqrt{\alpha^2 + 1}$  at  $\alpha = \sqrt{\alpha_0^2 - 1}$ . In physical case say electron emission where  $\alpha_0 = \frac{1}{\sqrt{4\pi\epsilon_0 G}} \frac{e}{m_e} = 2 \times 10^{21}$  is very large, it is equal to  $\alpha_0$ . It breaks down for  $\alpha < \alpha_0$ . For this range the transition line can be well approximated with  $\frac{Q}{M} = \sqrt{\alpha^2 + 1}$  same as the line specifying the extremal condition for black hole with mass above to solar mass. More accurate calculation bellow shows that the error in the above estimate is extremely small which becomes order of  $10^{-17}$  relatively near  $\alpha = \alpha_0$  for physical cases.

In order to evaluate  $\xi$  one can see from  $\frac{q}{m} \xi = \frac{dQ}{dM}$ , (2.19), and (2.20),

$$\xi = \frac{m}{q} \frac{dQ}{dM} = \frac{\int_m^\infty \frac{d\omega}{2\pi} \sum_{\text{mods } n} \frac{\gamma_n(\omega - \frac{qQ}{r_+})}{\exp((\omega - \frac{qQ}{r_+})/T_H) + 1} - \frac{\gamma_n(\omega + \frac{qQ}{r_+})}{\exp((\omega + \frac{qQ}{r_+})/T_H) + 1}}{\frac{1}{m} \frac{\partial M_{\text{neutral}}}{\partial t} + \int_m^\infty \frac{\omega}{m} \frac{d\omega}{2\pi} \sum_{\text{mods } n} \frac{\gamma_n(\omega - \frac{qQ}{r_+})}{\exp((\omega - \frac{qQ}{r_+})/T_H) + 1} + \frac{\gamma_n(\omega + \frac{qQ}{r_+})}{\exp((\omega + \frac{qQ}{r_+})/T_H) + 1}}, \quad (4.17)$$

here the term  $\frac{\partial M_{\text{neutral}}}{\partial t}$  presents contribution of other neutral particles which reduces  $\xi$ .

Obviously it can be seen that the above expression is always less than 1 ( $\xi < 1$ ).

For any given value of mass  $M$  and charge  $Q$  of the black hole and  $\alpha$  the value for  $\xi$  determines fate of the black hole or determines weather the black hole is in extremal regime or in decay regime. Indeed,  $\xi$  presents competition of charge and energy emission of the black hole.

We can estimate the integral in (4.17) as function of  $\frac{\omega}{T_H}(1 \pm \frac{qQ}{\omega r_+})$  by approximation, taking the peak value of the integrands at  $\omega = \omega_{max}$  and multiplying them by its effective width. Let us take  $\lambda = \frac{\omega_{max}}{T_H}$  and  $\eta = \frac{qQ}{\omega_{max} r_+}$ . According to figure 9 and [44],  $\omega_{max}$  increases as the temperature of the black hole increases ( $\omega_{max} \approx T_H$ ).  $\eta$  is small for the near extremal black holes for  $\alpha > 1$ , since  $T_H$  becomes very large. Then taking  $\eta$  small and neglecting the effect of neutral particles we have;

$$\begin{aligned} \xi &\lesssim \frac{\Delta\omega \sum_{mod\ n} \frac{\gamma_n(\lambda(1-\eta))}{\exp(\lambda(1-\eta))+1} - \frac{\gamma_n(\lambda(1+\eta))}{\exp(\lambda(1+\eta))+1}}{\Delta\omega \frac{\omega}{m} \sum_{mod\ n} \frac{\gamma_n(\lambda(1-\eta))}{\exp(\lambda(1-\eta))+1} + \frac{\gamma_n(\lambda(1+\eta))}{\exp(\lambda(1+\eta))+1}} \\ &\simeq -\lambda\eta \frac{\sum_{mod\ n} \gamma'_n(\lambda)}{\sum_{mod\ n} \gamma_n(\lambda)} - \lambda\eta \frac{1}{1+e^\lambda} + \lambda\eta. \end{aligned} \quad (4.18)$$

where  $\gamma'_n(\lambda) = \frac{\partial \gamma_n(\lambda)}{\partial \lambda}$ .

Hence the upper limit for  $\xi$  is given by  $\xi < \lambda\eta$  ( $\xi < \frac{qQ}{T_H r_+}$ ). As  $\omega_{max} \approx T_H$ , and  $\omega \geq m$ , for small black holes (black holes with high temperature or  $8\pi m M < 1$ ) we have  $T_H > m$ . Consequently these approximations leads to the following inequalities,

$$\xi < \frac{qQ}{T_H r_+} < \frac{qQ}{mr_+} < \frac{q}{m} \frac{1}{\sqrt{1+\alpha^2}}. \quad (4.19)$$

In order to calculate the transition line more precisely we assume the upper bound  $\xi < \frac{qQ}{T_H r_+}$  and insert it in (4.16).

$$\frac{4\pi q^2 Q}{m} \left(1 - \frac{r_-}{r_+}\right)^{\frac{\alpha^2-1}{\alpha^2+1}} < \frac{Q}{M} < \sqrt{1+\alpha^2}. \quad (4.20)$$

Or in another form,

$$\frac{4\pi q^2 \sqrt{r_- r_+}}{m} \frac{1}{\sqrt{1+\alpha^2}} \left(1 - \frac{r_-}{r_+}\right)^{\frac{\alpha^2-1}{\alpha^2+1}} < \frac{Q}{M} < \sqrt{1+\alpha^2}. \quad (4.21)$$

In order to obtain the transition line we put  $\frac{\xi q}{m} = \frac{Q}{M}$ .

$$\frac{4\pi q^2 Q}{m} \left(1 - \frac{r_-}{r_+}\right)^{\frac{\alpha^2-1}{\alpha^2+1}} = \frac{Q}{M}. \quad (4.22)$$

Numerical solution of this equation is given in figure 5. Solution of this equation gives us the transition line as a function of  $\alpha$ . Assuming  $\alpha \gg 1$ , the solution of the above equation gives,

$$\left. \frac{Q}{M} \right|_{Transition} = \frac{8\pi m M \alpha_0^2 / \alpha}{1 + 8\pi m M \alpha_0^2 / \alpha^2} \quad (4.23)$$

We see that this line decreases as a function of  $\alpha_0^2/\alpha$  at large  $\alpha$  as like as former approximation to transition line. Besides, contrary to the former approximation, this transition line does not intersect the boundary of  $r_- \leq r_+$  at  $\alpha = \alpha_0$ . For small  $\alpha \ll \alpha_0\sqrt{8\pi m M}$  this transition line is very close to the extremal boundary  $Q/M = \sqrt{\alpha^2 + 1}$  which is shown in figure 5. The relative difference to the extremal line for  $\alpha \gg 1$  is given by,

$$\frac{\sqrt{\alpha^2 + 1} - \frac{Q}{M}|_{Transition}}{\sqrt{\alpha^2 + 1}} \simeq \frac{1}{1 + 8\pi m M \alpha_0^2/\alpha^2} \quad (4.24)$$

In the system of standard units we assume that  $M_\odot = 2 \times 10^{30}$  as solar mass and for electron this distance becomes  $\frac{1}{1+4 \times 10^{59} \frac{M}{M_\odot} \frac{1}{\alpha^2}}$ . One can check that for small couplings this relative distance reduces to  $2.5 \times 10^{-60} \frac{M_\odot}{M} \alpha^2$ . Also at  $\alpha = \alpha_0$  this ratio becomes  $10^{-17}$ . This relative distance for a solar mass black hole and small  $\alpha$  shows that how much the black hole needs to be near the extremal limit to be in extremal regime. While for  $\alpha \gg \alpha_0\sqrt{8\pi m M}$  it reduces to 1 and covers all the  $0 < \frac{Q}{M} < \sqrt{\alpha^2 + 1}$  region.

One can compare this line with former approximation ( $\frac{Q}{M} = \alpha_0^2/\sqrt{\alpha^2 + 1}$ ). Both have similar behaviour as  $\alpha_0^2/\alpha$ . Hence, the ratio of their differences to the width of the region ( $\sqrt{\alpha^2 + 1}$ ) becomes,

$$\frac{\frac{\alpha_0^2}{\sqrt{\alpha^2 + 1}} - \frac{8\pi m M \alpha_0^2/\alpha}{1 + 8\pi m M \alpha_0^2/\alpha^2}}{\sqrt{\alpha^2 + 1}} \simeq \frac{1 + 8\pi m M \left( \frac{\alpha_0^2}{\alpha^2} - 1 \right)}{1 + 8\pi m M \alpha_0^2/\alpha^2} \frac{\alpha_0^2}{\alpha^2} \quad (4.25)$$

At  $\alpha > \alpha_0$ , as  $\alpha$  increases this ratio decreases and tends to zero. However, for large black holes where  $8\pi m M$  is greater than 1, it is possible that the above expression became negative (as explained before); the black hole becomes cooler and the inequality  $T_H > m$  no longer holds.

From our discussion in the first part of this section and numerical calculation of next section, we see that for  $\alpha > 1$  the backreaction and high potential barrier impedes the radiation near the extremal limit. Then the radiation vanishes; as a result, for the black holes in the extremal regime the final stage can be stable. Furthermore, at the limit  $\alpha \gg 1$  the background geometry tends to the flat one.

As the black hole tends to the extremal limit, its temperature increases and diverges, while its area vanishes. However, at this limit the potential barrier outside the event horizon of the black hole, as mentioned previously impedes the radiation of this hot body. Hence this potential barrier acting as an isolator outside the event horizon prevents the black hole to become in thermal equilibrium with outside world. Consequently, the black hole stays stable.



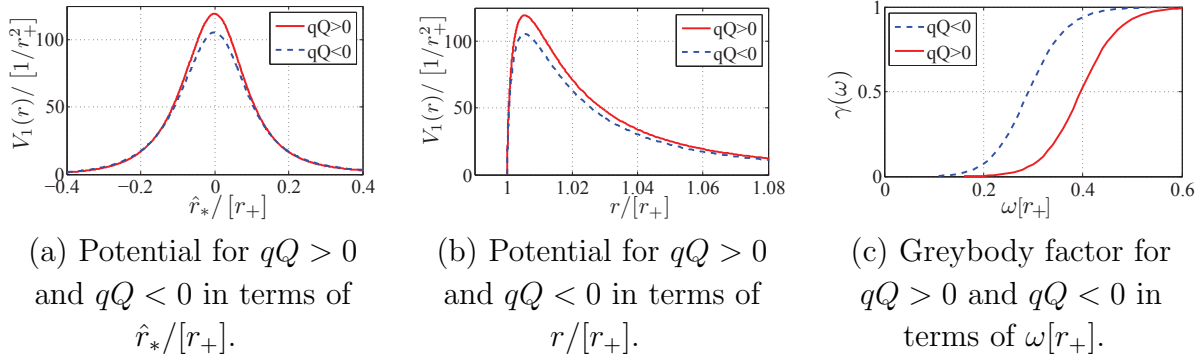


Figure 6: Dilaton black hole with parameters  $r_-/r_+ = 0.98$  and  $\alpha = 0.7$ . Charged spin  $\frac{1}{2}$  particles with  $\kappa = 1$ . Natural units and numerical values are  $G = \hbar = c = 4\pi\epsilon_0 = 1$ ,  $r_+ = 100$  and  $q[r_+] = 0.1$ .

## 5. Results and discussion

In this section we analyse and discuss effects of various parameters on the potential and greybody factors obtained in previous sections. Modification of the Hawking radiation on the light of the behaviour of the greybody factors is also discussed.

The discussion is based on numerical results in solving the basic equations (3.1). Since there are several parameters the discussion becomes complicated. So we discuss different factors separately.

We shall consider the effects of charge, mass and angular momentum of the emitted particle, dilaton coupling constant  $\alpha$ , the near extremal condition and finally the difference between scalars and fermions.

### 5.1. Effects of the charges of the emitted particle and of the black hole

The following analysis is based on computations leading to Figures 6a and 6b that show the potential barrier for both  $q$  having the same sign and opposite to the black hole.

It shows that the potential for the particles with the same signs as the black hole ( $qQ > 0$ ) is higher than the potential when the two signs are opposite ( $qQ < 0$ ). The result on the greybody factors can be seen in figure 6c which shows that for low frequencies ( $\omega r_+ \ll 1$  or more precisely  $\frac{\omega}{T_H} \ll 1$ ) the greybody factors for the same sign particles are always lower and hence less particles with the same sign are emitted at low frequencies i.e. they do not have sufficient energy to escape the barrier. The effect changes at high frequencies by including backreaction correction which can be seen from the figure 7d that shows the difference of the two greybody factors. When a high energy particle with opposite sign ( $qQ < 0$ ) is emitted, the black hole gets closer to the extremal limit and the height of potential barrier for  $\alpha > 1$  sharply increases. This higher potential barrier itself forces the emitted particle back toward the black hole.

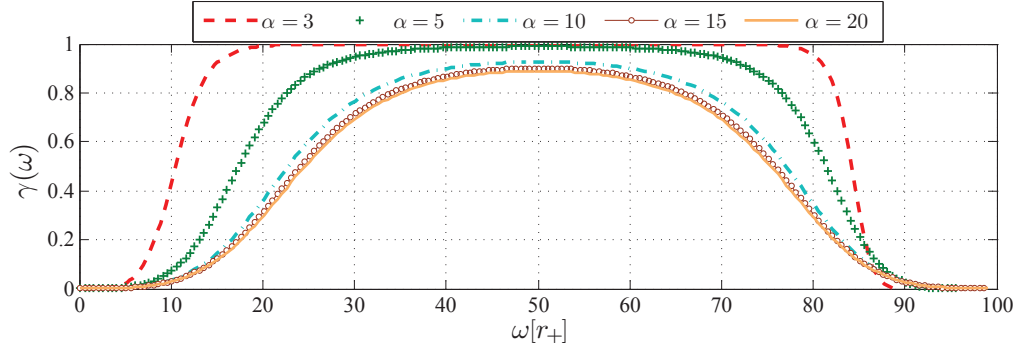
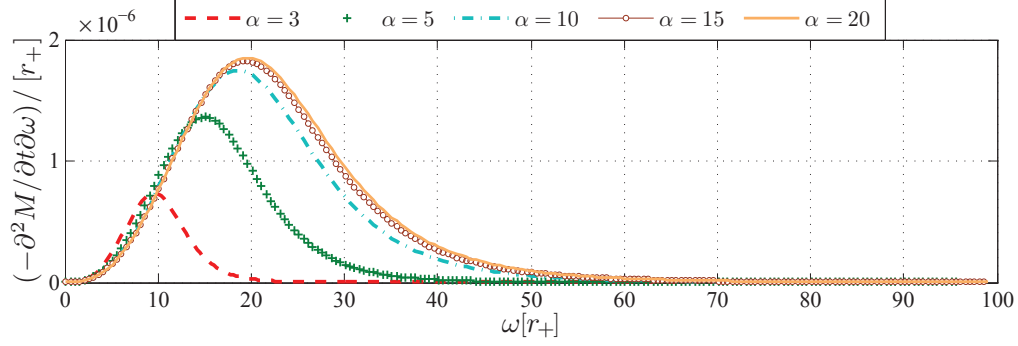
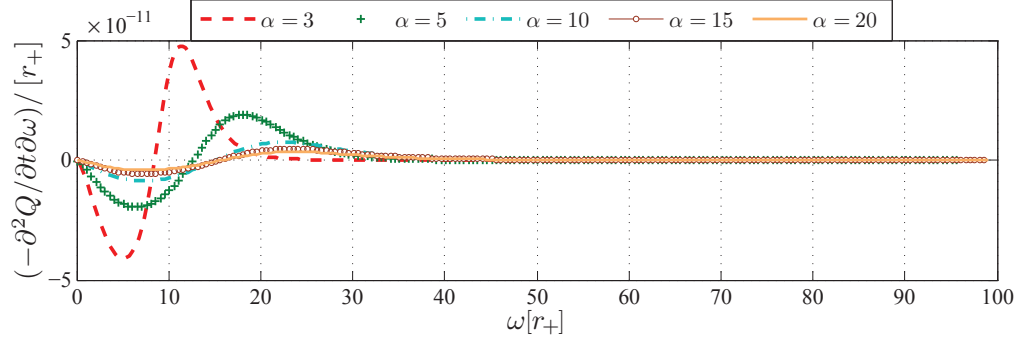
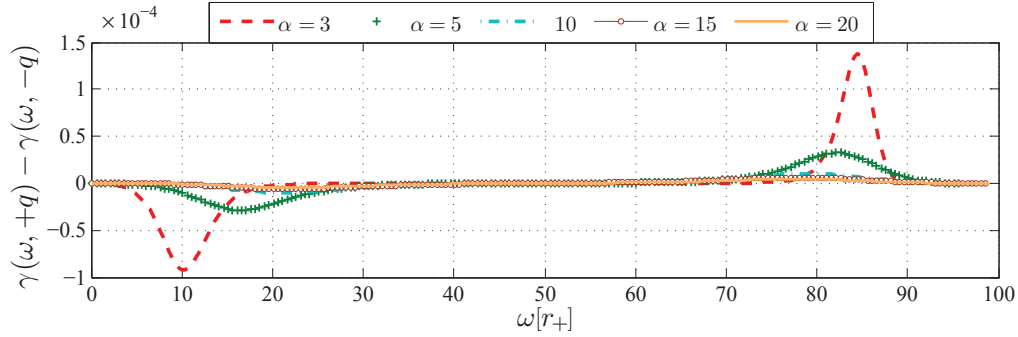
(a) Spectrum of greybody factors in terms of  $\omega[r_+]$ .(b) Spectrum of energy flux:  $F_E/[r_+] = -[r_+^{-1}]\partial M/\partial t$  in terms of  $\omega[r_+]$ .(c) Spectrum of charge flux:  $F_Q/[r_+] = -[r_+^{-1}]\partial Q/\partial t$  in terms of  $\omega[r_+]$ .(d) Subtraction of greybody factors for  $qQ > 0$  and  $qQ < 0$  in terms of  $\omega[r_+]$ .

Figure 7: Parameters are:  $r_-/r_+ = 0.98$ ,  $\alpha = 3, 5, 10, 15, 20$ ,  $\kappa = 1$ . Natural units and numerical values are  $G = \hbar = c = 4\pi\epsilon_0 = 1$ ,  $r_+ = 100$  and  $q[r_+] = 0.1$ .

Table 1: behaviour of maximum height  $V_{max}$ , location of maximum point  $r_{max}$  of effective potential,  $\gamma(\omega)$ , location of maximum point of power spectrum ( $\omega_{max}$ ) by increment of BH charge ( $\frac{r_-}{r_+} = (1 + \alpha^2) \frac{Q^2}{r_+^2} \nearrow 1$ ).

	$0 \leq \alpha < \frac{1}{\sqrt{3}}$	$\alpha = \frac{1}{\sqrt{3}}$	$\frac{1}{\sqrt{3}} < \alpha \leq 1$	$\alpha > 1$
$V_{max}$	$V_{max} \downarrow$	Does not change	$V_{max} \uparrow$	$V_{max} \nearrow \infty$
$r_{max}$	$r_{max} \nearrow \frac{2}{1+\alpha^2} r_+$	Does not change	$r_{max} \searrow \frac{2}{1+\alpha^2} r_+$	$r_{max} \searrow r_+$
$\gamma(\omega)$	$\gamma(\omega) \uparrow$	Does not change	$\gamma(\omega) \downarrow$	$\gamma(\omega) \downarrow$
$\omega_{max}$	$\omega_{max} \downarrow$	Does not change	$\omega_{max} \uparrow$	$\omega_{max} \uparrow$

Despite the fact that potential barrier prevents more of charged particles with same sign as the black hole than opposite sign particles to pass through, creation rate of charged particles with same sign to black hole due to thermal radiation is more than opposite sign particles. Hence, a competition arises between the thermal radiation and the greybody factors. At low energies particles cannot easily pass through the potential barrier hence the greybody factors will be dominant. On the other hand because high energy particles can pass through the potential barrier more easily, the thermal Hawking radiation will be dominant at high frequencies. As a result, at low frequencies sign of charge flux is opposite to the black hole charge, while at high frequencies it is equal. Exact calculations show that the total flux coming out of the black hole is always with the same sign of the black hole.

Figures 1, 8 and 9 show that as the charge of black hole increases, the radiation becomes more sensitive to the change of the coupling constant. On the other hand, at very low charges, the black hole behaves similar to the Reissner-Nordström black hole. In the range  $0 \leq \alpha < 1/\sqrt{3}$  as the charge of black hole increases the height of potential barrier decreases and the maximum recedes from the black hole resulting in the increase of the greybody factors and the location of the peak of the power spectrum  $\omega_{max}$  decreases. In the case  $\alpha = 1/\sqrt{3}$  the potential and greybody factors and  $\omega_{max}$  do not change with the change of the charge of the black hole. When  $1/\sqrt{3} < \alpha \leq 1$  the potential grows and its maximum moves toward the event horizon, the greybody factors decrease and  $\omega_{max}$  increases. At  $\alpha > 1$  and approaching the extremal limit, (3.22) shows that, the height of the potential grows indefinitely and the location of its maximum  $r_{max}$  approaches the event horizon, the greybody factors decrease and  $\omega_{max}$  increases. For a better understanding these results are shown on table 1.

The greybody factors as function of  $\omega$ , shows two low and high cutoff frequencies; the low cutoff does not show much sensitivity to different parameters including the charge. On the other hand the high cutoff frequency  $\omega_{HCF}$  shows strong dependence on  $\frac{r_-}{r_+} = (1 + \alpha^2) \frac{Q^2}{r_+^2}$ , which can be seen in figure 10a and equation (4.4) that shows it decreases as the charge increases.

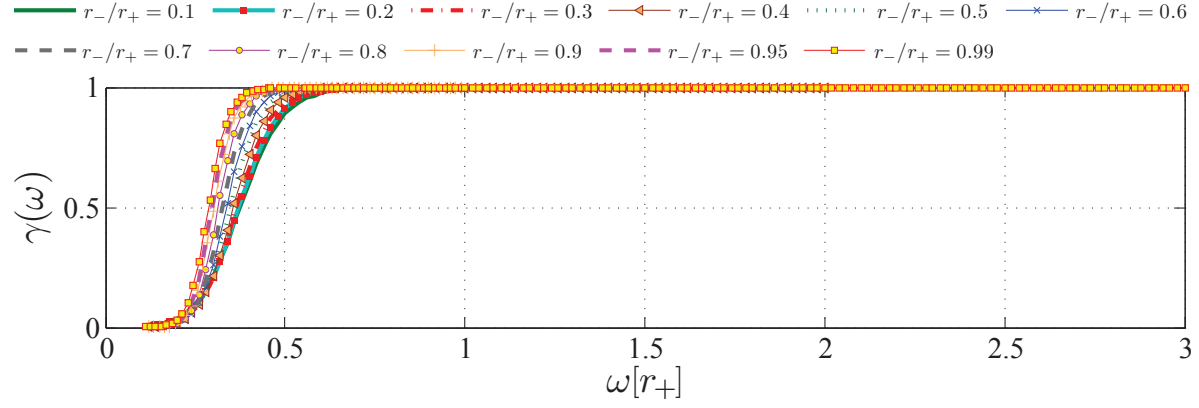
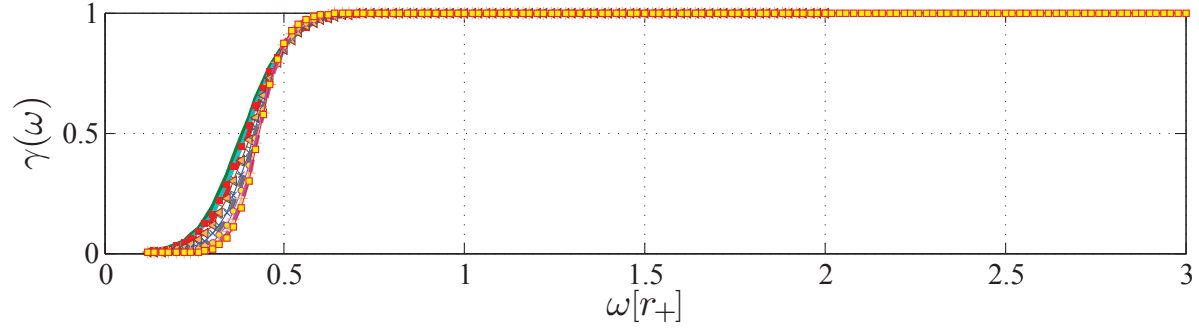
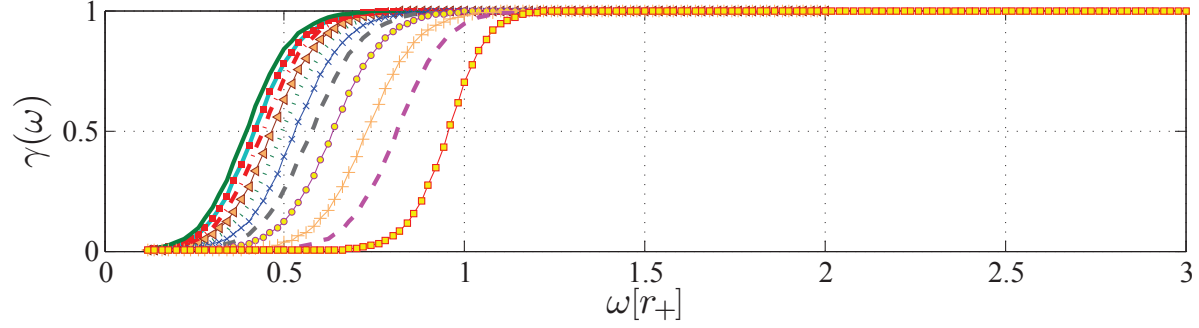
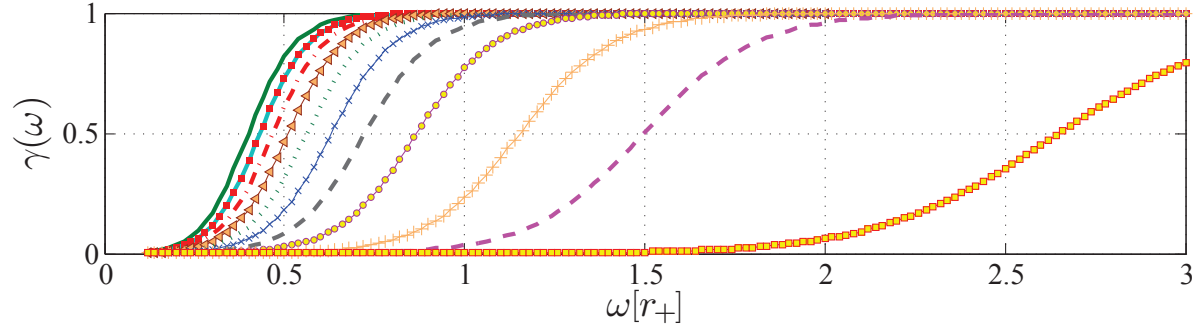
(a) Greybody factors of black hole with  $\alpha = 0$ .(b) Greybody factors of black hole with  $\alpha = 1/\sqrt{3}$ .(c) Greybody factors of black hole with  $\alpha = 1$ .(d) Greybody factors of black hole with  $\alpha = 1.4$ .

Figure 8

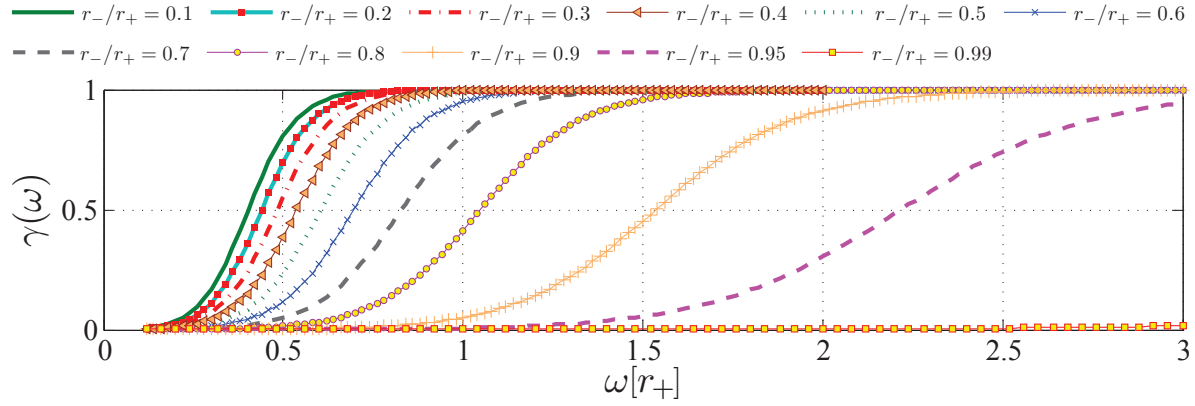
(e) Greybody factors of black hole with  $\alpha = \sqrt{3}$ .

Figure 8: Greybody factors of dilaton black hole with different values of  $\alpha$  and charge  $r_-/r_+ = (1 + \alpha^2) \frac{Q^2}{r_+^2}$  in terms of  $\omega[r_+]$ . Spin 1/2 particles with  $\kappa = 1$ . Natural units and numerical values are  $G = \hbar = c = 4\pi\epsilon_0 = 1$  and  $r_+ = 100$ .

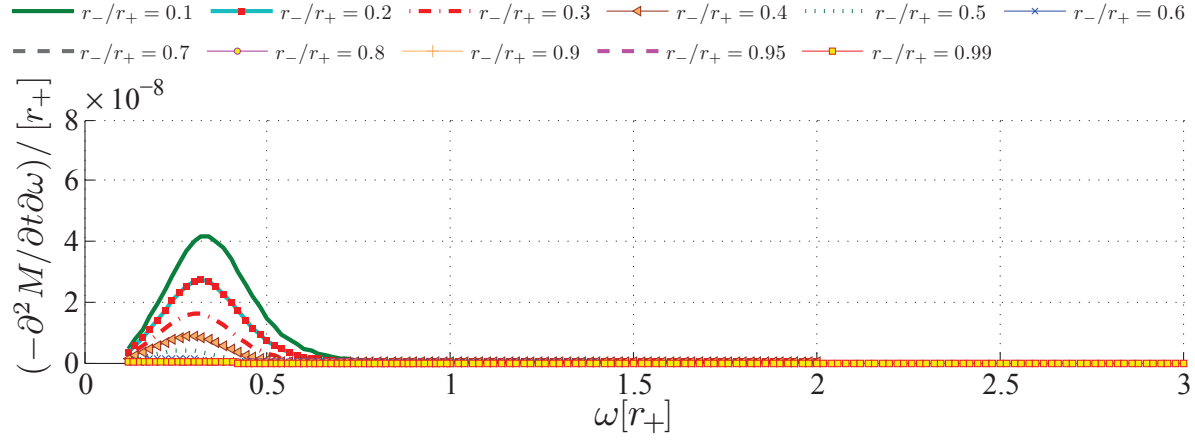
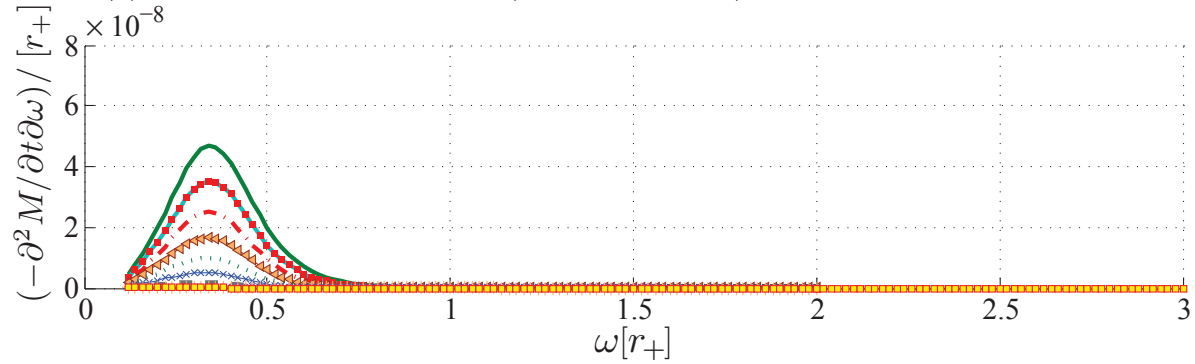
(a) Energy evaporation rates (power spectrum) of black hole with  $\alpha = 0$ .(b) Energy evaporation rates (power spectrum) of black hole with  $\alpha = 1/\sqrt{3}$ .

Figure 9

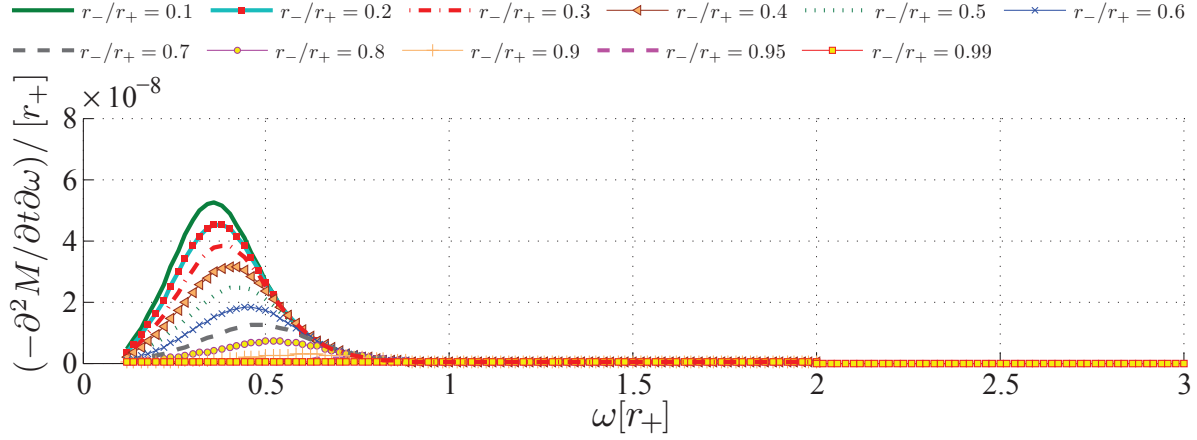
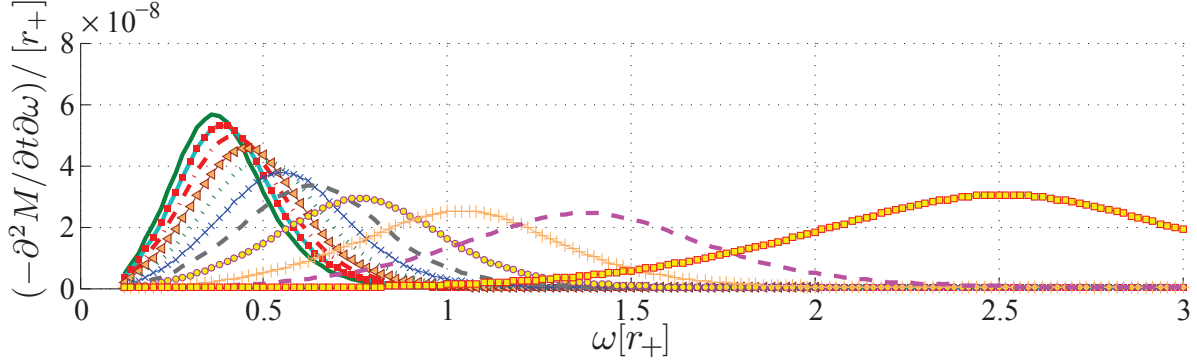
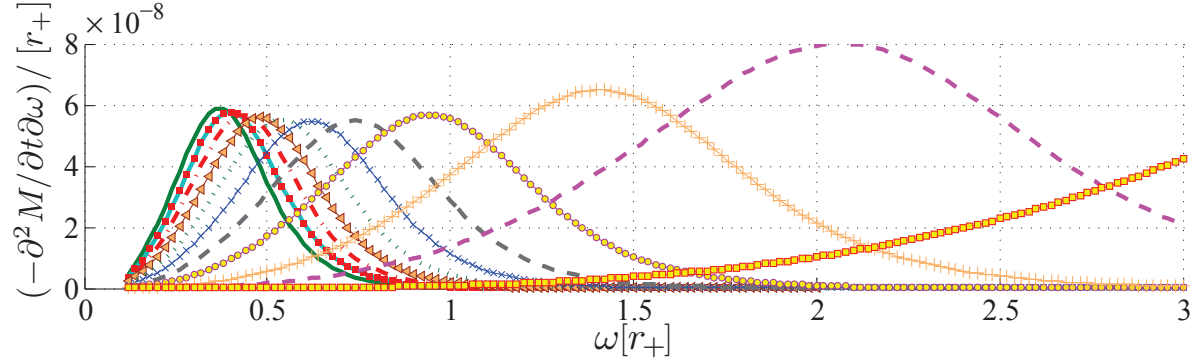
(c) Energy evaporation rates (power spectrum) of black hole with  $\alpha = 1$ .(d) Energy evaporation rates (power spectrum) of black hole with  $\alpha = 1.4$ .(e) Energy evaporation rates (power spectrum) of black hole with  $\alpha = \sqrt{3}$ .

Figure 9: Energy evaporation rates of dilaton black hole with different values of  $\alpha$  and charge ( $r_-/r_+ = (1 + \alpha^2) \frac{Q^2}{r_+^2} = 0.1, \dots, 0.99$ ) in terms of  $\omega[r_+]$ . Spin 1/2 particles with  $\kappa = 1$ . Natural units and numerical values are  $G = \hbar = c = 4\pi\epsilon_0 = 1$  and  $r_+ = 100$ .

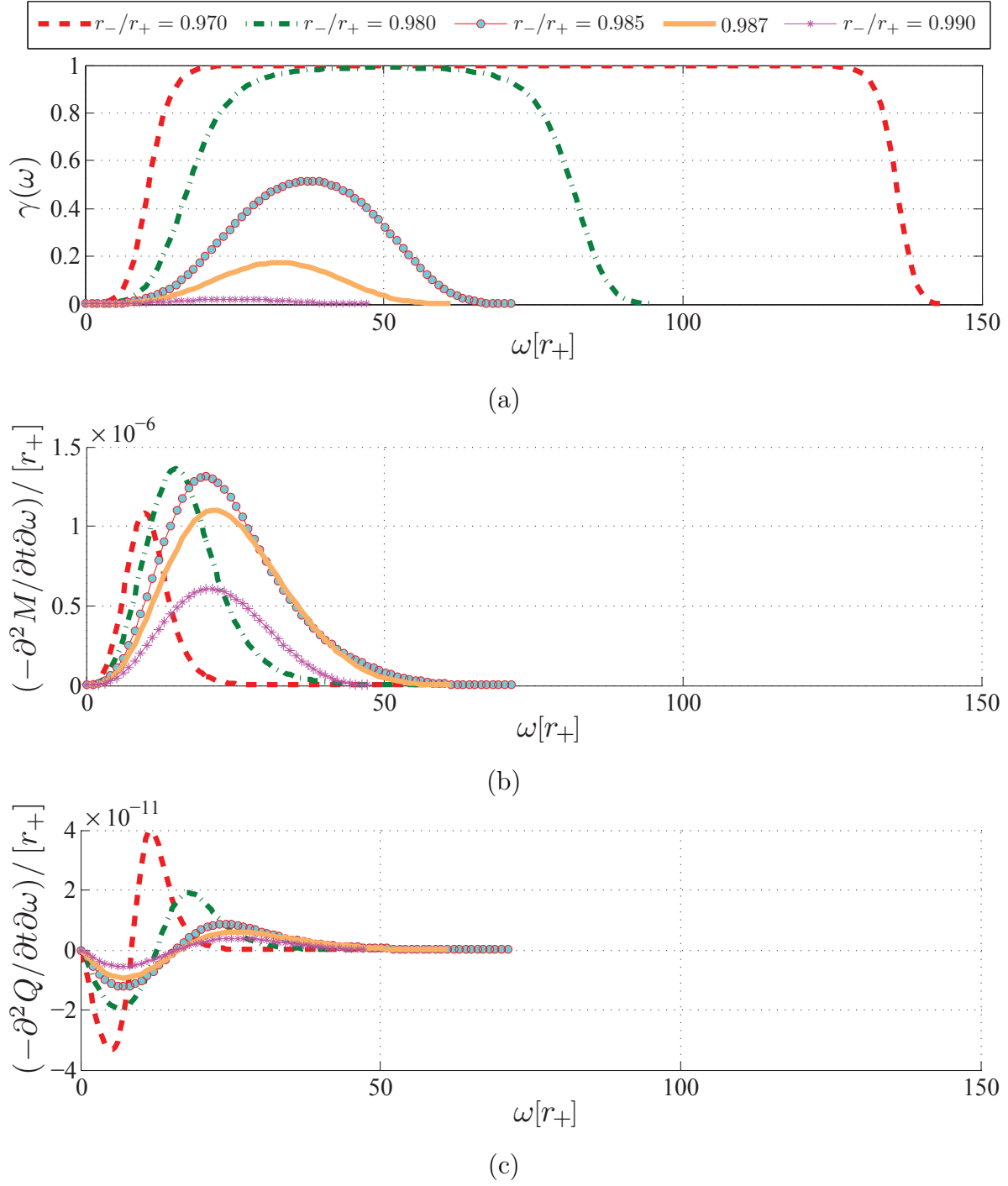


Figure 10: Spectrum of greybody factors  $\gamma(\omega, \kappa)$ , energy flux  $F_E/[r_+] = -[r_+^{-1}] \partial M / \partial t$  and charge flux  $F_Q/[r_+] = -[r_+^{-1}] \partial M / \partial t$  at the extremal limit with different values of charge ( $r_-/r_+ = (1 + \alpha^2) \frac{Q^2}{r_+^2} = 0.97, \dots, 0.99$ ) and with  $\alpha = 5$ , in terms of frequency  $\omega[r_+]$ . Particles with  $\kappa = 1$ . Natural units and numerical values are  $G = \hbar = c = 4\pi\epsilon_0 = 1$ ,  $r_+ = 100$  and  $q[r_+] = 0.1$ .

Table 2: behaviour of  $T_H$ ,  $-\frac{\partial M}{\partial t}$ ,  $-\frac{\partial Q}{\partial t}$ ,  $\omega_{HCF}$ , BW of  $-\frac{\partial M}{\partial t}$  and  $-\frac{\partial Q}{\partial t}$ , and  $\omega_{FCFS}$  by increment of BH charge ( $\frac{r_-}{r_+} = (1 + \alpha^2) \frac{Q^2}{r_+^2} \nearrow 1$ ).

-	$0 \leq \alpha < 1$	$\alpha = 1$	$\alpha > 1$
$T_H$	$T_H \searrow 0$	Does not change	$T_H \nearrow \infty$
$-\frac{\partial M}{\partial t}$	$-\frac{\partial M}{\partial t} \searrow 0$	$-\frac{\partial M}{\partial t} \downarrow$	First(low charge) $-\frac{\partial M}{\partial t} \downarrow$ then $-\frac{\partial M}{\partial t} \uparrow$
$-\frac{\partial Q}{\partial t}$	$-\frac{\partial Q}{\partial t} \searrow 0$	$-\frac{\partial Q}{\partial t} \downarrow$	First(low charge) $-\frac{\partial Q}{\partial t} \downarrow$ then $-\frac{\partial Q}{\partial t} \uparrow$
$\omega_{HCF}$	-	-	$\omega_{HCF} \searrow q/\sqrt{1+\alpha^2}$
Extremal limit	-	-	$-\frac{\partial Q}{\partial t} \rightarrow 0$ , $-\frac{\partial M}{\partial t} \rightarrow 0$
BW	$\text{BW} \searrow 0$	Does not change	$\text{BW} \uparrow$ (But at extremal limit $\text{BW} \rightarrow 0$ )
$\omega_{FCFS}$	-	-	$\omega_{FCFS} \uparrow$

The change in the Hawking temperature, as the charge changes depends on the value of  $\alpha$ .

For  $\alpha < 1$ , as  $Q$  increases the Hawking temperature decreases and approaches zero and the black hole cools, therefore the radiation is decreased (figures 9a, 9b and table 2).

For  $\alpha = 1$ , as  $Q$  increases the temperature  $T_H$  doesn't changes, greybody factors decrease, so evaporation rates decrease (figures 8c, 9c and table 2).

For  $\alpha > 1$  at small  $Q$ , the behaviour is similar to that of RN black hole. But as  $Q$  increases the Hawking temperature diverges and the black hole becomes hot, so the evaporation rates grows significantly with increase in the BW (bandwidth: the range covered between the two points where the evaporation rate is half of its maximum). FCFS (frequency of change in flux sign, i.e. the frequency where the sign of the charge flux is reversed,  $\omega_{FCFS}$ :  $-\frac{\partial^2 Q}{\partial t \partial \omega} \Big|_{\omega_{FCFS}} = 0$ ) also grows with the charge  $Q$  (figures 9d, 9e, 10c and table 2). However near the extremal limit due to presence of high cutoff frequency  $\omega_{HCF}$  the process slows and the emission rates and bandwidth get suppressed (figure 10 and table 2).

## 5.2. Effect of dilaton coupling constant

In the previous discussion on the effect of charge we have also discussed some of the effects of change in  $\alpha$ . In this part we look at changes in other quantities such as Hawking temperature, the emission rates, cutoff frequencies, ... as the dilaton coupling changes.

The special point  $\alpha = 1/\sqrt{3}$  which showed importance for charge dependence does not show any particular relevance for other quantities. On the other hand the particular point  $\alpha = 1$  marks serious changes in the behaviour of most of the quantities mentioned.



Table 3: behaviour of  $T_H$ ,  $V_{max}$ , width of potential,  $\gamma(\omega)$ ,  $-\frac{\partial M}{\partial t}$ ,  $-\frac{\partial Q}{\partial t}$ , bandwidth(BW) of  $-\frac{\partial M}{\partial t}$  and  $-\frac{\partial Q}{\partial t}$  and frequency of change in flux sign( $\omega_{FCFS}$ ) by increment of coupling constant  $\alpha$ .

	$\alpha \uparrow$
$T_H$	$T_H \uparrow$
$V_{max}$	$V_{max} \uparrow$
Width of potential	Decrease
$\gamma(\omega)$	$\gamma(\omega) \downarrow$
$-\frac{\partial M}{\partial t}$	$-\frac{\partial M}{\partial t} \uparrow$
$-\frac{\partial Q}{\partial t}$	$-\frac{\partial Q}{\partial t} \uparrow$ (But at the $\frac{1}{\sqrt{4\pi\epsilon_0 G}} \frac{e}{m_e} \frac{1}{\sqrt{1+\alpha^2}} \rightarrow 0$ limit tends to $-\frac{\partial Q}{\partial t} \rightarrow 0$ )
BW	BW $\uparrow$
$\omega_{FCFS}$	$\omega_{FCFS} \uparrow$

As the coupling constant increases, the height of the potential barrier shown in figure 1 increases along with a decrease in its width, which becomes considerable near extremal limit for  $\alpha > 1$ . In this case upon approaching the extremal limit, the height of the potential barrier grows indefinitely, and hence the greybody factors plotted in figures 11a and 11b decrease. In the limit of very large  $\alpha$  the dependence on  $\alpha$  disappears (figures 7 and 11). With increase in  $\alpha$ , the Hawking temperature of black hole increases. Hence the energy evaporation rate and its bandwidth shown in figure 11c increase and tends to a constant rate. Also the charge flux in figure 11d increases with  $\alpha$ , but as discussed in section 4.3 for  $\frac{e}{\omega} \frac{1}{\sqrt{1+\alpha^2}} \ll 1$  it decreases and tends to zero at the limit  $\frac{e}{\omega} \frac{1}{\sqrt{1+\alpha^2}} \rightarrow 0$ . The figure 7b shows the charge flux for different values of  $\alpha$ ; the change in the flux sign  $\omega_{FCFS}$ , occurs at a frequency which grows with  $\alpha$  due to increase of temperature. Table 3 gives a picture of the behaviour of the quantities with change in  $\alpha$ .

### 5.3. Effects of mass, angular momentum, and the statistic of the emitted particle

Again the quantity to study is the height of the potential that has strong effect on the greybody factors. Equation (3.15) shows the height of potential barrier grows as the angular momentum of particle increases. Increase of the angular momentum  $\kappa$ , causes considerable decrease in the energy and charge fluxes. This is why it is rational to consider only the lowest value of the angular momentum, in the case of our interest  $\kappa = 1$ .

Equation (4.14) shows that the mass of the particle affects the low frequency spectrum of greybody factors. Particles with energy less than the rest mass  $\omega \leq m$  are not real and will never reach the infinity and hence the relevant greybody factors vanish and with that, the energy and charge fluxes.

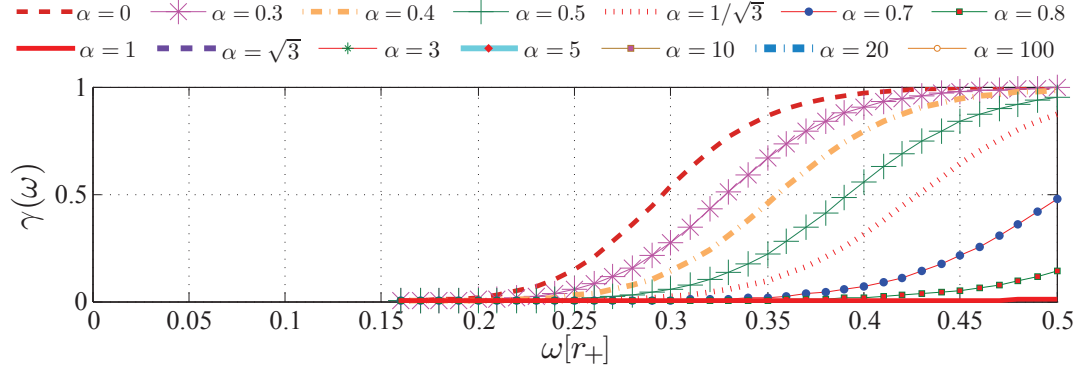
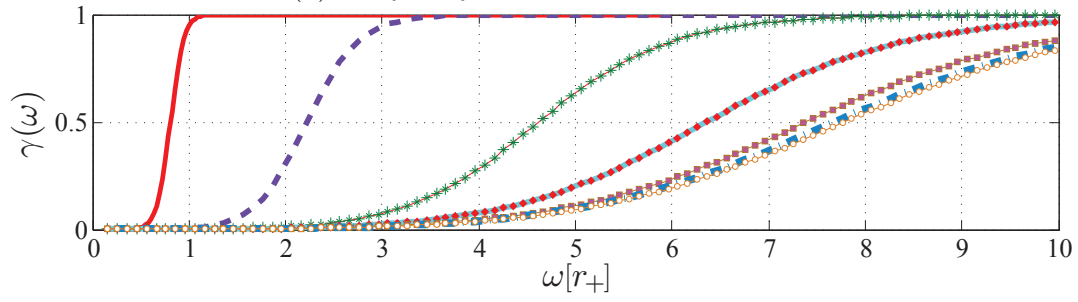
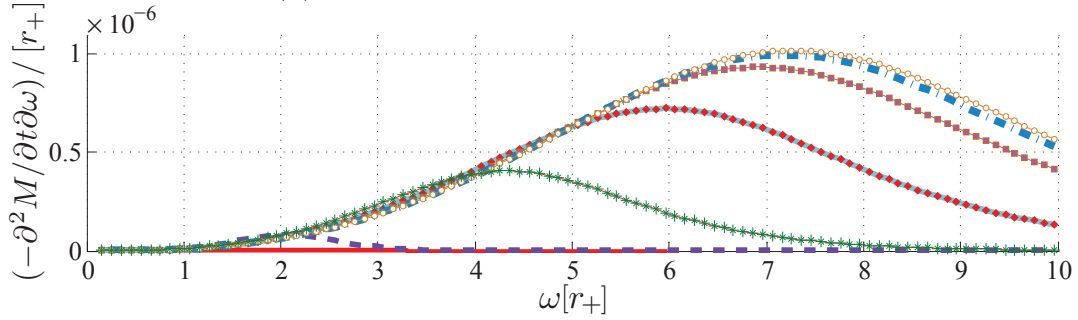
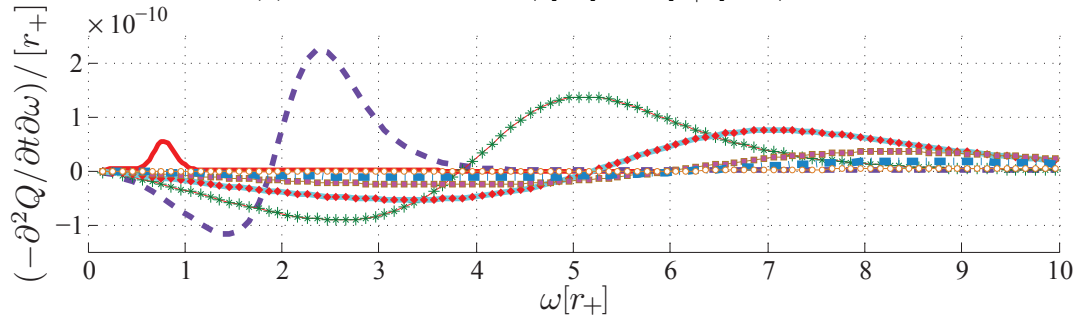
(a) Greybody factors for  $\alpha = 0, \dots, 1$ .(b) Greybody factors for  $\alpha = 1, \dots, 100$ .(c) Energy fluxes  $F_E/[r_+] = -[r_+^{-1}]\partial M/\partial t$ .(d) Charge fluxes  $F_Q/[r_+] = -[r_+^{-1}]\partial Q/\partial t$ .

Figure 11: Greybody factors (a), (b) and energy (c) and charge (d) evaporation rates of dilaton black hole with different values of  $\alpha$  with  $r_-/r_+ = 0.95$  in terms of frequency  $\omega[r_+]$ . Spin 1/2 particles with angular momentum  $\kappa = 1$ . Natural units and numerical values are  $G = \hbar = c = 4\pi\epsilon_0 = 1$ ,  $r_+ = 100$  and  $q[r_+] = 0.1$ .

The effective potential obtained for spin 1/2 particles behaves like the scalar particle potential which is mentioned in section 2 and calculated in [3]. For the class  $\alpha < 1$ , at the event horizon the potential barrier vanishes. This barrier has a finite maximum tending to zero by increasing radius. For the case  $\alpha = 1$ , the height of potential barrier near the extremal limit remains finite. For  $\alpha > 1$ , in the extremal limit the height of potential barrier diverges while its position approaches the event horizon. For non-extremal cases the height of potential barrier is finite, but its peak (as it tends to extremal limit) grows as like as  $(r_+ - r_-)^{-2(\alpha^2-1)/(\alpha^2+1)}$ .

Figure 2 shows that the height and width of the effective potentials for scalars are smaller than effective potentials for fermions and greybody factors and hence evaporation rates for scalars are always greater than greybody factors and evaporation rates for fermions.

However, the overall behaviour of dilaton black hole for scalar particles on increasing or decreasing parameters  $\alpha$  and  $Q$  is similar to fermions, the scalar particles dominate over the fermions on determining the fate of dilaton black hole.

## 6. Conclusion

In this paper we have calculated the greybody factors for charged spin 1/2 particles in the dilaton black hole background and investigated its effects. First it was done using the Rosen-Morse potential and WKB approximation. The advantage of these methods are that they gave us a good general formula that described the behaviour of greybody factors albeit approximately. In calculation of evaporation rates by Rosen-Morse method errors become significant. To avoid these errors we performed more accurate numerical computations. Although qualitatively, and for most of the time even quantitatively these analytic computations are reliable. In the calculation of evaporation rates semi-classical approximation was employed. For better accuracy we applied back-reaction correction. This correction, adiabatically brought the dynamics into the solution which shows a considerable effect on high frequency spectrum of the greybody factors especially near extremal limit. Consideration of the backreaction caused highly non-trivial picture which specially revealed new phenomenon of evaporating to extremal limit as fate of certain dilaton black holes. We obtained a cutoff frequency for greybody factors at high frequency for  $\alpha > 1$ . Hence greybody factors act like filter i.e. filter for low and high frequencies, like a band-pass filter. With the increase of the charge of the black hole high cutoff frequency  $\omega_{HCF}$  decreases, while low cutoff frequency  $\omega_{LCF}$  increases. As a result in this limit the black hole stops radiating.

We obtained that for  $\alpha > 1$  due to the growth and divergence of the temperature and height of the potential barrier of the black hole, a competition between these two arises. For low charges the greybody factors are dominant (as the charge of black hole increases the evaporation rate decreases) while for large  $Q$  the temperature takes over

(as the charge of the black hole increases the evaporation rates increases). Also increase of the coupling constant acts in favor of the temperature; as  $\alpha$  increases the onset of the increase of the evaporation rate moves to lower charges. This effect does not last forever, at the extremal limit due to the existence of high cutoff frequency the radiation become suppressed. Divergence of low cutoff frequency and decrease in high cutoff frequency at the extremal limit turn off the Hawking radiation of the black hole. In this situation from viewpoint of an infinite observer the space-time around the event horizon of the black hole extinguishes the Hawking radiation of dilaton black hole.

We also obtained another difference that distinguishes dilaton black hole from other black holes. Because the charge evaporation rate is always faster than the energy evaporation rate normal black holes always lose their charge and become neutral, and then, similar to the Schwarzschild black hole radiate their energy away and disappear. But for the dilaton black holes we have found unexpected result that fate of the black hole depends on different variables,  $Q/M$ ,  $\alpha$ ,  $mM$ , and  $\alpha_0 = q/m$  charge over mass ratio of the emitted particle. A transition line separates the two regions in the  $(Q/M, \alpha)$  plane.

For the first approximation, we obtained this transition line to be  $Q/M = \alpha_0^2/\sqrt{\alpha^2 + 1}$  for  $\alpha > \sqrt{\alpha_0^2 - 1}$ . This approximation gave an upper bound for  $\xi$  for small black holes ( $8\pi mM < 1$ ). More precise solution of this transition line shows that there is a small area of extremal regime for  $\alpha < \sqrt{\alpha_0^2 - 1}$ . Precise solution shows that for  $\alpha < \alpha_0\sqrt{8\pi mM}$  a tiny part of the allowed region belongs to the extremal regime and almost all of it belongs to the decay regime. In contrast for  $\alpha > \alpha_0\sqrt{8\pi mM}$  a much larger part of the allowed space belongs to the extremal regime. Therefore for small black holes, in practice  $\alpha_0$  marks a critical value for  $\alpha$  below which almost all the conditions result in total evaporation and after which most of the parameter space belongs to the extremal regime.

In the extremal regime the final state of the black hole is a stable situation where it acts like an elementary particle [3]. Incidentally for this region the background metric become flat as the temperature tends to infinity and its entropy vanishes; stabilizing the black hole which makes it more identifiable with an elementary particle.

During the radiation process the greybody factors always tend to add charge to the black hole in contrast with Hawking radiation spectrum that always tends to discharge it. Now the question is why this competition is always in the interest of the Hawking radiation and not the greybody factors. The answer to this question is that the gravity where the Hawking radiation originates, near the event horizon is stronger than the effect of the greybody factors which have their source outside the event horizon.

The fate of an extremal dilaton black hole may differ from the Reissner-Nordström black hole, in the  $\alpha = 1$  case, since the role of the two horizons in the charged dilaton black hole are very different. Evolution of rotating dilaton black holes and corresponding transition line may differ from the non rotating case and needs a separate analysis. It may be possible that at large  $\alpha$  we may be able to consider a class of these black

holes as elementary particles; being stable and possessing definite mass, spin and charge. Throughout this work we have always considered  $r_- < r_+$ . The case for  $r_- > r_+$  is very different and also needs its own particular analysis. These questions are under investigation by the authors.

## Acknowledgments

We would like to thank Navid Abbasi for fruitful discussions and reading the manuscript.

## Appendix

In this appendix charged massive Dirac equation in the background of most general spherically symmetric static black hole is changed into Schrödinger like equation by appropriate change of variables. The methods developed in [20–23, 28, 30, 36–38] are employed.

Consider the most general spherically symmetric static metric

$$ds^2 = A(r)^2 dt^2 - B(r)^2 dr^2 - C(r)^2 d\Omega^2. \quad (\text{A.1})$$

Dirac equation with charge  $q$  and mass  $m$  in the background metric is given by [21, 28],

$$(i\gamma^\mu D_\mu - m)\Psi = 0. \quad (\text{A.2})$$

where

$$D_\mu = \partial_\mu + \Gamma_\mu - iqA_\mu, \quad (\text{A.3})$$

where  $A_\mu$  is the Maxwell field and  $\Gamma_\mu$  the spin connection defined by

$$\Gamma_\mu = \frac{1}{8} [\gamma^a, \gamma^b] e_a^\nu e_{b\nu;\mu}, \quad (\text{A.4})$$

$e_\mu^a$  is the tetrad,

$$e_\mu^a = \text{diag}(A(r), B(r), C(r), C(r) \sin \theta). \quad (\text{A.5})$$

Contraction  $\gamma^\mu \Gamma_\mu$  in Dirac equation gives

$$\gamma^\mu \Gamma_\mu = \gamma^r \frac{1}{4B(r)} \left( \frac{1}{A(r)^2} \frac{\partial A(r)^2}{\partial r} + \frac{2}{C(r)^2} \frac{\partial C(r)^2}{\partial r} \right) + \gamma^\theta \frac{1}{2C(r)} \cot \theta. \quad (\text{A.6})$$

Inserting (A.6) in Dirac equation and taking  $A_\mu = (A_t, 0, 0, 0)$  we obtain

$$\left\{ i \frac{\gamma^t}{A(r)} (\partial_t - iqA_t) + i \frac{\gamma^r}{B(r)} \left( \partial_r + \frac{1}{4A(r)^2} \frac{\partial A(r)^2}{\partial r} + \frac{1}{2C(r)^2} \frac{\partial C(r)^2}{\partial r} \right) \right. \\ \left. + i \frac{\gamma^\theta}{C(r)} \left( \partial_\theta + \frac{1}{2} \cot \theta \right) + i \frac{\gamma^\varphi}{C(r) \sin \theta} \partial_\varphi - m \right\} \Psi = 0. \quad (\text{A.7})$$

With definition of  $\Psi = A(r)^{-\frac{1}{2}}(\sin \theta)^{-\frac{1}{2}}\Phi$  [20, 36] and substitution into (A.7) gives

$$\left\{ i \frac{\gamma^t}{A(r)} (\partial_t - iqA_t) + i \frac{\gamma^r}{B(r)} \left( \partial_r + \frac{1}{2C(r)^2} \frac{\partial C(r)^2}{\partial r} \right) + i \frac{\gamma^\theta}{C(r)} \partial_\theta + i \frac{\gamma^\varphi}{C(r) \sin \theta} \partial_\varphi - m \right\} \Phi = 0. \quad (\text{A.8})$$

In order to remove angular terms let us define the operator  $K$

$$K = \gamma^t \gamma^r \gamma^\theta \frac{\partial}{\partial \theta} + \gamma^t \gamma^r \gamma^\varphi \frac{1}{\sin \theta} \frac{\partial}{\partial \varphi}. \quad (\text{A.9})$$

Hence we obtain

$$\left\{ i \frac{\gamma^t}{A(r)} (\partial_t - iqA_t) + i \frac{\gamma^r}{B(r)} \left( \partial_r + \frac{1}{C(r)} \frac{\partial C(r)}{\partial r} \right) - i \frac{\gamma^r \gamma^t}{C(r)} K - m \right\} \Phi = 0. \quad (\text{A.10})$$

Introducing the ansatz

$$\Phi = \begin{pmatrix} \frac{iG^{(\pm)}(r)}{C(r)} \phi_{jm}^{(\pm)}(\theta, \varphi) \\ \frac{F^{(\pm)}(r)}{C(r)} \phi_{jm}^{(\mp)}(\theta, \varphi) \end{pmatrix} e^{-i\omega t}, \quad (\text{A.11})$$

with

$$\phi_{jm}^+ = \begin{pmatrix} \sqrt{\frac{l+1/2+m}{2l+1}} Y_l^{m-1/2} \\ \sqrt{\frac{l+1/2-m}{2l+1}} Y_l^{m+1/2} \end{pmatrix}, \quad (\text{A.12})$$

for  $j = l + 1/2$

and

$$\phi_{jm}^- = \begin{pmatrix} \sqrt{\frac{l+1/2-m}{2l+1}} Y_l^{m-1/2} \\ -\sqrt{\frac{l+1/2+m}{2l+1}} Y_l^{m+1/2} \end{pmatrix}. \quad (\text{A.13})$$

for  $j = l - 1/2$

Eigenvalues of  $K$  by applying on ansatz are obtained as follows

$$\kappa_{(\pm)} = \begin{cases} (j + \frac{1}{2}) & j = l + \frac{1}{2}, \\ -(j + \frac{1}{2}) & j = l - \frac{1}{2}. \end{cases} \quad (\text{A.14})$$

Here  $\kappa_{\pm}$  is positive and negative integers ( $\kappa_{\pm} = \pm 1, \pm 2, \dots$ ).

With simplification we get

$$\begin{cases} \frac{1}{A(r)} (\omega + qA_t) G^{(\pm)}(r) + \frac{1}{B(r)} \frac{\partial}{\partial r} F^{(\pm)}(r) + \frac{1}{C(r)} \kappa_{(\pm)} F^{(\pm)}(r) - m G^{(\pm)}(r) = 0, \\ -\frac{1}{A(r)} (\omega + qA_t) F^{(\pm)}(r) + \frac{1}{B(r)} \frac{\partial}{\partial r} G^{(\pm)}(r) - \frac{1}{C(r)} \kappa_{(\pm)} G^{(\pm)}(r) - m F^{(\pm)}(r) = 0. \end{cases} \quad (\text{A.15})$$

Introducing tortoise coordinate  $r_* = \int (B(r)/A(r)) dr$ , the radial equations for  $F^{(\pm)}$  and  $G^{(\pm)}$  become

$$\begin{aligned} \frac{d}{dr_*} \begin{pmatrix} F^{(\pm)}(r) \\ G^{(\pm)}(r) \end{pmatrix} - A(r) \begin{pmatrix} -\frac{\kappa_{(\pm)}}{C(r)} & m \\ m & \frac{\kappa_{(\pm)}}{C(r)} \end{pmatrix} \begin{pmatrix} F^{(\pm)}(r) \\ G^{(\pm)}(r) \end{pmatrix} \\ = \begin{pmatrix} 0 & -(\omega + qA_t) \\ (\omega + qA_t) & 0 \end{pmatrix} \begin{pmatrix} F^{(\pm)}(r) \\ G^{(\pm)}(r) \end{pmatrix}. \end{aligned} \quad (\text{A.16})$$

Defining  $\hat{F}^{(\pm)}$  and  $\hat{G}^{(\pm)}$  by

$$\begin{pmatrix} \hat{F}^{(\pm)} \\ \hat{G}^{(\pm)} \end{pmatrix} = \begin{pmatrix} \sin(\theta_{(\pm)}/2) & \cos(\theta_{(\pm)}/2) \\ \cos(\theta_{(\pm)}/2) & -\sin(\theta_{(\pm)}/2) \end{pmatrix} \begin{pmatrix} F^{(\pm)} \\ G^{(\pm)} \end{pmatrix}, \quad (\text{A.17})$$

with

$$\theta_{(\pm)} = \text{arccot}(\kappa_{(\pm)} / mC(r)), \quad 0 \leq \theta_{(\pm)} \leq \pi. \quad (\text{A.18})$$

Applying (A.17) into (A.16) gives

$$\frac{\partial}{\partial \hat{r}_*} \begin{pmatrix} \hat{F}^{(\pm)} \\ \hat{G}^{(\pm)} \end{pmatrix} + W_{(\pm)} \begin{pmatrix} -\hat{F}^{(\pm)} \\ \hat{G}^{(\pm)} \end{pmatrix} = \omega \begin{pmatrix} \hat{G}^{(\pm)} \\ -\hat{F}^{(\pm)} \end{pmatrix}, \quad (\text{A.19})$$

Equation (A.19) can be easily separated. So with definition of  $V_{(\pm)1,2} = W_{(\pm)}^2 \pm \partial W_{(\pm)} / \partial \hat{r}_*$  and for simplification removing  $(\pm)$  we get

$$\frac{\partial^2}{\partial \hat{r}_*^2} \hat{F} + (\omega^2 - V_1) \hat{F} = 0, \quad (\text{A.20})$$

$$\frac{\partial^2}{\partial \hat{r}_*^2} \hat{G} + (\omega^2 - V_2) \hat{G} = 0, \quad (\text{A.21})$$

where

$$V_{1,2} = W^2 \pm \frac{\partial W}{\partial \hat{r}_*}, \quad (\text{A.22})$$

and

$$W = A(r) \left( m^2 + \frac{\kappa^2}{C(r)^2} \right)^{\frac{1}{2}} \left( 1 + \frac{q}{\omega} A_t + \frac{1}{2} \frac{A(r)}{B(r)} \frac{\frac{m}{\omega} \kappa}{(\kappa^2 + m^2 C(r)^2)} \frac{\partial C(r)}{\partial r} \right)^{-1}, \quad (\text{A.23})$$

In (A.21) following change of variable is applied

$$\hat{r}_* = \int \frac{B(r)}{A(r)} \left( 1 + \frac{q}{\omega} A_t + \frac{1}{2} \frac{A(r)}{B(r)} \frac{\frac{m}{\omega} \kappa}{(\kappa^2 + m^2 C(r)^2)} \frac{\partial C(r)}{\partial r} \right) dr. \quad (\text{A.24})$$

This new coordinate is obtained from tortoise coordinate  $r_* = \int (B(r)/A(r)) dr$ . Hence, we call this coordinate *generalized tortoise coordinate* change.

In studying the black holes with anisotropic metric factors like Lifshitz, where we have anisotropic scale transformation, understanding the effect of these factors is critically important, so we calculated the effective potential for most general spherically symmetric static family of black hole.

Considering the superpotential  $W$  we see that the factor of metric  $A(r)$  can have crucial effect on potential with respect to the factor  $B(r)$ . Hence for the black holes which factor  $A(r)$  has a distinct behaviour we can expect different results.

## References

- [1] G. W. Gibbons and K. -i. Maeda, Nucl. Phys. B **298** (1988) 741.

- [2] D. Garfinkle, G. T. Horowitz and A. Strominger, Phys. Rev. D **43** (1991) 3140 [Erratum-ibid. D **45** (1992) 3888].
- [3] C. F. E. Holzhey and F. Wilczek, Nucl. Phys. B **380** (1992) 447 [hep-th/9202014].
- [4] J. -i. Koga and K. -i. Maeda, Phys. Rev. D **52** (1995) 7066 [hep-th/9508029].
- [5] S. W. Hawking, Commun. Math. Phys. **43** (1975) 199 [Erratum-ibid. **46** (1976) 206].
- [6] G. W. Gibbons, Commun. Math. Phys. **44** (1975) 245.
- [7] J. M. Bardeen, B. Carter and S. W. Hawking, Commun. Math. Phys. **31** (1973) 161.
- [8] D. N. Page, Phys. Rev. D **16** (1977) 2402.
- [9] M. Cvetič and F. Larsen, Phys. Rev. D **57** (1998) 6297 [hep-th/9712118].
- [10] P. Kanti and J. March-Russell, Phys. Rev. D **67** (2003) 104019 [hep-ph/0212199].
- [11] S. Creek, O. Efthimiou, P. Kanti and K. Tamvakis, Phys. Rev. D **76** (2007) 104013 [arXiv:0707.1768 [hep-th]].
- [12] S. Das and A. Dasgupta, JHEP **9910** (1999) 025 [hep-th/9907116].
- [13] S. S. Gubser, Phys. Rev. D **56** (1997) 7854 [hep-th/9706100].
- [14] U. A. al-Binni and G. Siopsis, Phys. Rev. D **79** (2009) 084041 [arXiv:0902.2194 [hep-th]].
- [15] M. O. P. Sampaio, JHEP **0910** (2009) 008 [arXiv:0907.5107 [hep-th]].
- [16] M. Casals, S. R. Dolan, P. Kanti and E. Winstanley, JHEP **0703** (2007) 019 [hep-th/0608193].
- [17] M. O. P. Sampaio, JHEP **1002** (2010) 042 [arXiv:0911.0688 [hep-th]].
- [18] G. W. Gibbons and M. Rogatko, Phys. Rev. D **77** (2008) 044034 [arXiv:0801.3130 [hep-th]].
- [19] L. Nakonieczny and M. Rogatko, Phys. Rev. D **84** (2011) 044029 [arXiv:1108.3892 [hep-th]].
- [20] S. Chen, B. Wang and R. Su, Class. Quant. Grav. **23** (2006) 7581 [gr-qc/0701089].
- [21] H. T. Cho, Phys. Rev. D **68** (2003) 024003 [gr-qc/0303078].
- [22] H. T. Cho and Y. -C. Lin, Class. Quant. Grav. **22** (2005) 775 [gr-qc/0411090].
- [23] H. T. Cho, A. S. Cornell, J. Doukas and W. Naylor, Phys. Rev. D **75** (2007) 104005 [hep-th/0701193].
- [24] S. K. Chakrabarti, Eur. Phys. J. C **61** (2009) 477 [arXiv:0809.1004 [gr-qc]].
- [25] C. Doran, A. Lasenby, S. Dolan and I. Hinder, Phys. Rev. D **71** (2005) 124020 [gr-qc/0503019].
- [26] S. Dolan, C. Doran and A. Lasenby, Phys. Rev. D **74** (2006) 064005 [gr-qc/0605031].
- [27] W. M. Jin, Class. Quant. Grav. **15** (1998) 3163 [gr-qc/0009009].
- [28] J. -I. Jing, Phys. Rev. D **69** (2004) 084009 [gr-qc/0312079].
- [29] J. -I. Jing, Phys. Rev. D **70** (2004) 065004 [gr-qc/0405122].
- [30] J. Jing, Phys. Rev. D **72** (2005) 027501 [gr-qc/0408090].
- [31] E. Jung, S. Kim and D. K. Park, JHEP **0409** (2004) 005 [hep-th/0406117].
- [32] A. Lopez-Ortega, Gen. Rel. Grav. **37** (2005) 167.
- [33] A. Lopez-Ortega, Rev. Mex. Fis. **56** (2010) 44 [arXiv:1006.4906 [gr-qc]].
- [34] A. Lopez-Ortega and I. Vega-Acevedo, Gen. Rel. Grav. **43** (2011) 2631 [arXiv:1105.2802 [gr-qc]].
- [35] R. Moderski and M. Rogatko, Phys. Rev. D **77** (2008) 124007 [arXiv:0805.0665 [hep-th]].
- [36] R. Sini, N. Varghese and V. C. Kuriakose, arXiv:0802.0788 [gr-qc].
- [37] F. -W. Shu and Y. -G. Shen, Phys. Rev. D **70** (2004) 084046 [gr-qc/0410108].
- [38] C. -Y. Wang, Y. Zhang, Y. -X. Gui and J. -B. Lu, arXiv:0910.5128 [gr-qc].
- [39] C. Eckart, Phys. Rev. **35** (1930) 1303.
- [40] N. Rosen and Philip M. Morse, Phys. Rev. **42** (1930) 210.
- [41] P. Boonserm and M. Visser, JHEP **03** (2011) 073 [arXiv:1005.4483 [hep-th]].
- [42] J. Preskill, P. Schwarz, A. D. Shapere, S. Trivedi and F. Wilczek, Mod. Phys. Lett. A **6** (1991) 2353.
- [43] J. -I. Koga and K. -I. Maeda, Phys. Lett. B **340** (1994) 29 [hep-th/9408084].
- [44] J. M. Maldacena and A. Strominger, Phys. Rev. D **55** (1997) 861 [hep-th/9609026].
- [45] T. Harmark, J. Natario and R. Schiappa, Adv. Theor. Math. Phys. **14** (2010) 727 [arXiv:0708.0017 [hep-th]].
- [46] P. Kraus, gr-qc/9508007.
- [47] S. -B. Chen and J. -L. Jing, Class. Quant. Grav. **22** (2005) 1129.



- [48] H. T. Cho, A. S. Cornell, J. Doukas, T. R. Huang and W. Naylor, *Adv. Math. Phys.* **2012** (2012) 281705 [arXiv:1111.5024 [gr-qc]].
- [49] V. Cardoso and J. P. S. Lemos, *Phys. Rev. D* **67** (2003) 084020 [gr-qc/0301078].
- [50] R. A. Konoplya and A. Zhidenko, *Rev. Mod. Phys.* **83** (2011) 793 [arXiv:1102.4014 [gr-qc]].
- [51] A. Nagar, O. Zanotti, J. A. Font and L. Rezzolla, *Phys. Rev. D* **75** (2007) 044016 [gr-qc/0610131].